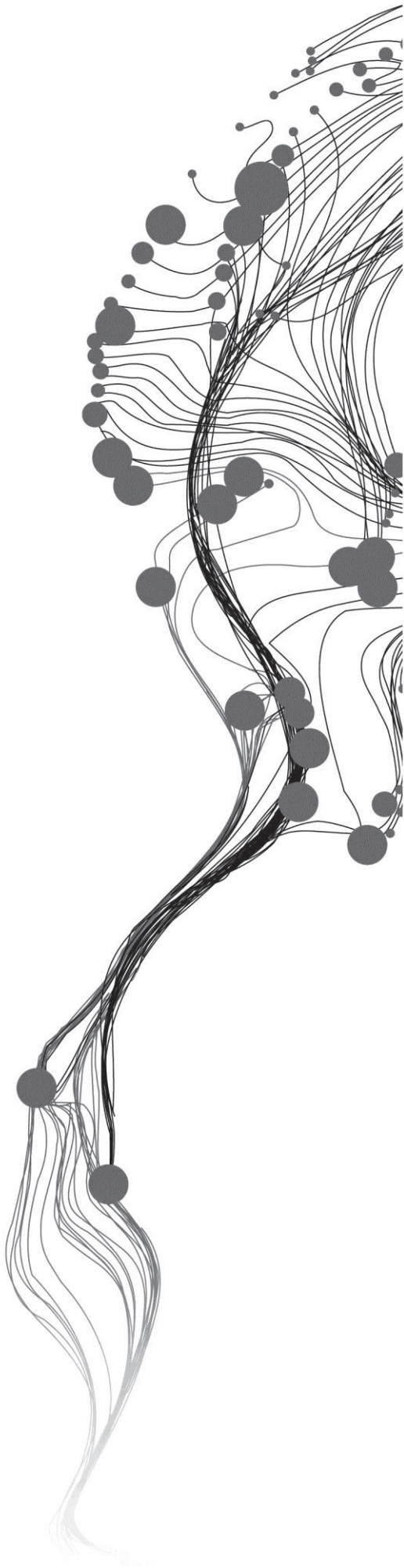


Assessment of Drought Early Warning in Ethiopia

*A comparison of WRSI by surface energy balance and
soil water balance*

Melaku Estifanos Abraha
March, 2013

SUPERVISORS:
Dr Ir. Chris Mannaerts
Dr Ir. Joris Timmermans



Assessment of Drought Early Warning in Ethiopia

*A comparison of WRSI by surface energy balance and
soil water balance*

Melaku Estifanos Abraha
Enschede, The Netherlands, March, 2013

Thesis submitted to the Faculty of Geo-Information Science and Earth
Observation of the University of Twente in partial fulfilment of the
requirements for the degree of Master of Science in Geo-information Science
and Earth Observation.

Specialization: Water Resource and Environmental Management

SUPERVISORS:

Dr Ir. Chris Mannaerts

Dr Ir. Joris Timmermans

THESIS ASSESSMENT BOARD:

Prof. Dr. Z. Bob Su (Chair)

Dr Ir. C.A.J.M. Kees de Bie (External Examiner) ITC Natural Resources

DISCLAIMER

This document describes work undertaken as part of a programme of study at the Faculty of Geo-Information Science and Earth Observation of the University of Twente. All views and opinions expressed therein remain the sole responsibility of the author, and do not necessarily represent those of the Faculty.

ABSTRACT

Drought is a natural disaster causing adverse impacts on vegetation, animals, and people. Drought is generally considered as a deficiency of rainfall or increase in evapotranspiration over a prolonged period of time. Although it is equally severe in all parts of the world, its impact is more pronounced when it occurs in developing countries where rain-fed agriculture is the major economic base. In Ethiopia, drought occurs frequently and forms the major natural hazard. In many parts of the country, agricultural productions are characterized by significant fluctuations due to variation in moisture availability and this in turn lead to crop failure and widespread drought.

This research entails to study the water requirement of three major crops and to evaluate the occurrence of drought in a semi-arid region of northern Ethiopia, where rainfall is unreliable and unpredictable.

Different meteorological and satellite based drought indices are currently available for monitoring and analysis of drought over a specified period of time. In this research, water requirement satisfaction index (WRSI) is used to examine the spatial distribution of drought and crop performance based on the availability of water during a growing season. In Ethiopia, LEAP has been implemented to estimate WRSI for assessing drought and early warning. However, its standard output lacks temporal and spatial details. As a result, accurate assessment of drought remains a difficult task. This study therefore aims to improve the accuracy of drought assessment by comparing WRSI estimates from soil water balance and energy balance approaches.

The study was conducted in Tigray, northern Ethiopia, where drought is a recurrent phenomenon. Evapotranspiration was estimated based on soil water balance and energy balance approaches to understand the occurrence and extent of drought. Geostationary satellite products and ground based meteorological data were employed to estimate WRSI for the three major rain-fed crops in the study area. The findings of the study reveal that water balance method can provide reasonable estimates of actual crop evapotranspiration distribution for rain-fed crops, which aids accurate drought assessment.

The findings on comparison between SEBS AET and LSA SAF AET indicated a similar spatial and temporal distribution with a good correlation (> 0.5) for the three major crops studied. Thus it can be inferred that LSA SAF AET can provide a reliable AET estimate for proper assessment of drought in near real time. The WRSI determined using GEONETcast and in-situ data at station level clearly indicated that water balance model is strongly dependent on rainfall and higher WRSI values were observed in areas with high rainfall distribution. The findings further revealed that WRSI estimates based on the energy balance approach can provide appropriate estimates of WRSI for proper monitoring of drought early warning during cloud free days. However, during existence of cloud cover, water balance method is an appropriate alternative for drought monitoring.

Keyword:-Drought assessment, Water Requirement satisfaction index, Water balance and energy balance Crop evapotranspiration, GEONETcast, Reference evapotranspiration

ACKNOWLEDGEMENTS

First and foremost I am everlastingly thankful to the almighty God for giving me his grace, support and strength to finish my work.

I am very much indebted to my first supervisor Dr. Ir. Chris Mannaerts for his support, critical comments, and suggestions throughout the study. His guidance, comments and suggestions were fruit full to bring my work in to completion. His door is open and always welcome for me when I face a problem during the research.

My deepest gratitude also goes to my second supervisor Dr Ir. Joris Timmermans for his immense support, constructive comments. His simulating suggestions and guidance were productive and I learnt a lot from them.

I would like to thank the Government of Netherlands and to the faculty of Geo-information science and Earth observation (ITC) university of Twente for financing my scholarship. I would like to extend my special thanks to Tigray bureau of water resource, Tigray bureau of agriculture and rural development and national meteorological agency Tigray brunch for their cooperation during my field work for data collection.

My special thanks also go to my beloved family my mother Kiros Reta, my sister Eyerusalem Estifanos my late father Abraha Estifanos and others for their courage nonstop assistance to be strong and patient in life. Especially my late father Abraha I cannot express your endless support throughout my life.

I would like to express my heartfelt and loving thanks to my beloved friend Saba Yohanness and her family for their help, courage and condolence during my difficult time. Sabi it is because of your help, courage and love that I am here.

Especial thanks to my friend Dr. Tagel Gebrehiwot for his advice and support during my stay in ITC and during my thesis work.

Finally I would like to thank all my friends for their courage and moral support that made my stay in Netherlands memorable. Kiflom, Abraham, Asmelash Kahsu, Rishan and others I will always remember the time we spend together with a smile. My grateful thanks also goes to my friends back home Gebrehaweria Gebrekirstos, Asrat kahsay, Solomon Tadesse, Selam, wedi Amare, Wedi Arbea (Mehari Negash), Micheale Gebremedhin, Berihu Teklehymanot, Tesfamichael Zemichael, Goshu Gebrehiwot with his family, my friend since my childhood Teshale Afework, and others for their moral support and condolence during my previous sorrow time.

Last but not least I would to thank all the staff members of the department of Water Resource and Environmental Management for sharing us with their appreciated knowledge during our study at ITC and to my classmates for sharing their knowledge and experiences during my stay.

TABLE OF CONTENTS

Abstract	i
Acknowledgements	ii
List of figures	v
List of tables	vi
List of Abbreviations	vii
List of Symbols	ix
1. Introduction.....	1
1.1. Background.....	1
1.1.1. Drought Assessment	1
1.1.2. GEONETcast	2
1.2. Research Problems	2
1.3. Research Objectives	3
1.3.1. Specific Objectives.....	3
1.4. Research Questions.....	3
2. Literature Review.....	5
2.1. Drought.....	5
2.1.1. Types of drought.....	5
2.1.2. Drought in Ethiopia	5
2.1.3. Drought Indices	6
2.2. Water Requirement Satisfaction Index	6
2.3. Water Balance Concept	7
2.4. Evapotranspiration Concepts.....	7
2.4.1. The Surface Energy Balance System.....	8
2.5. Concept of GEONETcast	8
3. Study Area.....	11
3.1. Location and administration divisions	11
3.2. Agro-ecological zonation	12
3.3. Climate.....	12
3.4. Landuse and Landcover	12
3.5. Drought Situation.....	13
4. Data Collection	15
4.1. Ground observation data	15
4.1.1. IN-situ Data.....	15
4.1.2. Land Cover Data.....	15
4.2. Crop specific data.....	16
4.2.1. Crop Coefficient and Crop Calendar.....	16
4.3. Meteorological Data.....	17
4.3.1. European Centre for Medium-Range Weather Forecasts	18
4.4. Satellite Data.....	18
4.4.1. Tropical Applications of Meteorology using Satellites.....	19
4.4.2. Satellite Application Facility for Land Surface Analysis	19
5. Methods.....	21
5.1. Estimation of Crop Water Requirement	22
5.1.1. Estimating Reference Evapotranspiration	23
5.2. Estimating AET from Soil Water Balance Model	23
5.3. Precipitation.....	25

5.3.1. Reliability of Gauge Rainfall data	25
5.3.2. Comparison of TAMSAT Rainfall with In-situ Rainfall	25
5.4. Estimating AET from SEBS	27
5.4.1. Comparing AET from SEBS with Land SAF AET.....	29
5.5. Comparing WRSI from SEBS with Water Balance.....	29
6. Results and Discussion	31
6.1. Rainfall reliability analysis for gauge stations in the study area	31
6.2. Validation of TAMSAT Rainfall Data	32
6.3. Estimation of Actual Evapotranspiration from Water Balance	33
6.4. Comparison of AET from SEBS and LSA SAF	35
6.5. Comparison of WRSI from Soil water Balance and Energy Balance	38
7. Conclusions and Recommendation.....	41
7.1. Conclusion	41
7.2. Recommendation	42
List of References.....	43
List of appendices.....	47
Appendix-A	47
Appendix-B.....	50
Appendix-C	53
Appendix-D.....	54
Appendix-E	55

LIST OF FIGURES

Figure 1-1: General structure of the thesis	4
Figure 2-1:-GEONETcast global coverage.....	9
Figure 3-1:-Location Map of the study area	11
Figure 3-2:-Agro-ecological zone based on altitude, BOFED 2002	12
Figure 3-3:- Land cover map of Tigray	13
Figure 4-1:-Major rain fed crops growing in the study area.....	16
Figure 4-2:-Kc values for the major crops in the area taken from LEAP.....	16
Figure 4-3:-Ethiopian major food crop calendar.....	17
Figure 4-4:-Total weather stations available in the study area.....	17
Figure 5-1:-WRSI flow chart	21
Figure 5-2:-Total in situ (left) and satellite (right) rainfall of the area for 2012 growing season.....	25
Figure 5-3:-Water Balance Flow Chart	26
Figure 5-4:-Energy Balance Flow Chart.....	30
Figure 6-1:-Total rainfall stations of the study area.....	32
Figure 6-2:-Pixel to pixel (left) and point to pixel (right) Comparison of TAMSAT rainfall with in- situ rainfall for September	33
Figure 6-3:- AET trend for Teff in the western (upper left), central (upper right), eastern (lower left) and southern (lower right) parts in relation to ETc and ET0	34
Figure 6-4 :- Spatial distribution of AET for three major crops.....	35
Figure 6-5:-Trend of AET from SEBS and LSA SAF for barley (a), wheat (b) and Teff (c)	37
Figure 6-6:-Comparison of SEBS AET with LSA SAF AET for barley (upper left), wheat (upper right) and Teff (lower left) stations.....	38
Figure 6-7:-Spatial distribution of WRSI for barley, wheat and Teff (left to right) derived from soil water balance (upper) and energy balance (lower)	39

LIST OF TABLES

Table 4-1:-Description of different data sets used in this study	15
Table 4-2:-Currently Working Synoptic Meteorological stations.....	18
Table 5-1:-Kc and root depth fraction of the three major crops in the study area	23
Table 6-1:-Evaluating the reliability of rainfall stations	31
Table 6-2:-Point to pixel and pixel to pixel comparison results of rainfall data.....	32

LIST OF ABBREVIATIONS

A.S.L	Above Sea Level
BOFED	Bureau of Finance and Economic Development
CMA	Chines Meteorological Administration
CMI	Crop Moisture Index
CSA	Central Statistical Authority
DRMFSS	Disaster Risk Management and Food Security Sector
DSLFL	Down welling Surface Long wave Flux
DSSF	Down welling Surface Short wave Flux
ECMWF	European Centre for Medium rage Weather Forecasting
EM	Emissivity
ENSO	El Niño and Southern Oscillation
EO	Earth Observation
EOS	End of season
EPS	EUMETSAT polar system
ESA	European Space Agency
ETDI	Evapotranspiration Deficit Index
ET0	Reference Evapotranspiration
EUMETSAT	European Meteorological Satellites
FAO	Food and Agricultural organization
FVC	Fraction of Vegetation Cover
GEO	Global Earth Observation
GEOSS	Global Earth Observation System of Systems
GPS	Ground Positioning System
IDW	Inverse Distance Weighting Method
IOD	Indian Ocean Dipole
LAI	Leaf Area Index
LEAP	Livelihood Early Assessment Protection
LGP	Length of Growing Period
LSASAF	Land Surface Analysis Satellite Application Facility
LST	Land Surface Temperature
MSG	Meteosat Second Generation
MODIS	Moderate Resolution imaging Spectroradiometer
NESDIS	National Environmental Satellite Data and Information Service
NDVI	Normalized Difference Vegetation Index
NMA	National Meteorological Agency
NOAA	National Oceanic and Atmospheric Administration
NWP	Numerical Weather Prediction
PDSI	Palmer Drought Severity Index
PHDI	Palmer Hydrologic Drought Index
PSNP	Productive Safety Net Program
RDI	Reclamation Drought Index
RFE	Rainfall Estimates
RMSE	Root Mean Square Error
SEBS	Surface Energy Balance Systems
SMDI	Soil Moisture Drought Index

SOS	Start of Season
SPI	Standard Precipitation Index
SST	Sea Surface Temperature
SWSI	Surface water Supply Index
TAMSAT	Tropical Application of Meteorological Satellites
TIR	Thermal Infrared
UNWFP	United Nations World Food Programme
USDA	United States Department of Agriculture
WMO	World Meteorological Organization
WR	Water Requirement
WRSI	Water requirement Satisfaction Index

LIST OF SYMBOLS

Symbols	Description	Unit
AET	Actual Crop Evapotranspiration	[mm day ⁻¹]
ETc	Crop water requirement	[mm day ⁻¹]
ET0	Reference Evapotranspiration	[mm day ⁻¹]
R _a	Extraterrestrial radiation	[MJ m ⁻² day ⁻¹]
R _n	Net Radiation at the crop surface	[MJ m ⁻² day ⁻¹]
e_s	Saturation Vapour Pressure	[kPa]
e_a	Actual vapour pressure	[kPa]
$e_s - e_a$	Saturation vapour pressure deficit	[kPa]
G ₀	Soil heat flux	[MJ m ⁻² day ⁻¹]
T _a	Air temperature	[°C]
R _s	Solar or shortwave radiation	[MJ m ⁻² day ⁻¹]
R _s	Solar radiation	[MJ m ⁻² day ⁻¹]
R _{swd}	Incoming shortwave radiation	[W m ⁻²]
R _{lwd}	Incoming long wave radiation	[W m ⁻²]
R _{so}	Clear-sky radiation	[MJ m ⁻² day ⁻¹]
PAW	plant available water	[mm]
WHC	Water Holding Capacity	[mm]
σ	Stefan-Boltzmann constant	[MJ K ⁻⁴ m ⁻² day ⁻¹]
PPT	Decadal precipitation	[mm]
RD _f	Root depth fraction	[m]
SW _f	Average fraction of WHC	[mm]
SW _i	Soil water content at the end of the i th time interval	[mm decadal ⁻¹]
k	Von Karman's constant	[-]
u	Wind speed	[m s ⁻¹]
θ_0	Potential temperatures at the surface	[°C]
u_*	Friction velocity	[m s ⁻¹]
Z _{0h}	Roughness height for heat transfer	[m]
Z _{0m}	Roughness height for momentum transfer	[m]
d ₀	Displacement height	[m]

Ψ_m	Stability correction function for momentum	[-]
Ψ_h	Stability correction heat transfer	[-]
θ_v	Mean virtual temperature	[°C]
g	Acceleration due to gravity	[m s ⁻²]
q	Specific humidity	[kg kg ⁻¹]
r_i	Bulk surface internal resistance	[s ⁻¹]
r_e	Aerodynamic resistance	[s ⁻¹]
SW _{i-1}	Initial soil water content at the beginning of the growing season	[mm]
α_o	surface albedo	[-]
ε	Emissivity of the surface	[-]
R_{lwd}	Outgoing long wave radiation and	[W m ⁻²]
T_o	land surface temperature	[°K]
Δ	Slope of vapour pressure curve	[K pa °C ⁻¹]
γ	Psychometric constant	[K pa °C ⁻¹]
G_{sc}	solar constant	[-]
d_r	inverse relative distance Earth-Sun	[rad]
ω	Sunset hour angle	[rad]
ϕ	Latitude	[rad]
δ	Solar declination angle	[rad]
P	Air pressure	[Pa]
K_c	Crop coefficient	[]
H	Sensible heat at	[W m ⁻²]
Γ_s and Γ_c	proportions of heat fluxes	[-]
Λ	Evaporation fraction	[-]
KB^{-1}	Excess resistance to heat transfer	[-]
λ	Latent heat of vaporization	[kJ kg ⁻¹]

1. INTRODUCTION

1.1. Background

Drought

Drought is a natural environmental hazard causing adverse impacts on vegetation, animals, and people (Edossa et al., 2010). In recent years, it has been occurring frequently in all climatic zones and significantly affects crop yields causing shortage of food as well as animal forage when it occurs (Boken, 2009). Drought is generally defined as a deficiency of rainfall or increase of evapotranspiration over prolonged period of time. Such precipitation regimes are directly influenced by different climatic effects such as EL-Nino. According to Haile (1988), an increase in sea surface temperature in the central and equatorial Pacific Ocean and southern oscillation (SO) leads to a change in atmospheric pressure across the pacific basin. With climate change this results in an imbalance between precipitation, evaporation, and transpiration. Combined effect of El Niño and Southern Oscillation (ENSO) results in air and ocean phenomenon with global weather implications often associate with devastating droughts.

1.1.1. Drought Assessment

Assessing drought development is crucial for accurate quantification and monitoring of its socio-economic impacts (Boken, 2009). Traditional methods of drought assessment that depend on rainfall data from local stations in general do not express much spatial detail and are difficult to obtain at near-real time. In contrast, drought monitoring tools based on satellite data are consistently available in near real time and can be used to identify the start of drought, its duration and magnitude prior to harvests. The use of satellite derived drought indices can lead to better drought prediction (Ataklti, 2012).

Reviews of literature reveal that vegetation indices developed using band combination of satellite imagery have been used for monitoring drought since mid-1990s. Despite a range of vegetation indices based on remote sensing have been used to monitor drought, the Normalized Difference Vegetation Index (NDVI) from NOAA's was the most commonly used to estimate drought indices like Evapotranspiration Deficit Index (ETDI) and Soil Moisture Drought Index (SMDI). However combinations of different vegetation indices, land surface parameters, and precipitation data will provide even better drought predictions (Ataklti, 2012).

In that context, the Livelihood Early Assessment Protection (LEAP) was developed by World Food Program's (WFP's) Ethiopia drought insurance project in 2006. It was developed as a spatial assessment tool for drought early warning to guide disbursements from contingent funds for a Productive Safety Net Program (PSNP) scale-up during drought. LEAP integrates rainfall estimates, evapotranspiration, and soil water content as the main input to simulate growth and crop water requirements through the growing season. It is a grid based model working for Ethiopia at 10km * 10km resolution data and the product acquires a 10-day synthesis. Nevertheless, due to high rainfall variability in the country and coarse spatial resolution of the LEAP model, assessing early warning and drought monitoring accurately is difficult (Ataklti, 2012; Gelassie, 2012). Thus, accurate drought monitoring demands a single crop assessment method which requires near real time with relatively higher spatial resolution data. In this aspect remote sensing data from GEONET cast plays a huge role for accurate assessment of drought (Gelassie, 2012).

1.1.2. GEONETcast

GEONETcast is a tool that provides local, regional and global datasets in near-real-time through satellite communication system (Maathuis et al., 2008). It supports the GEO societal benefit areas in which environmental observations are transmitted directly to the end user through satellites. It is a global environmental information delivery technique used to transmit satellite and in-situ data products through satellite communication.

The European Organization for the Use of Meteorological Satellites (EUMETSAT), the United States National Oceanic and Atmospheric Administration (NOAA), and the Chins Meteorological Administration (CMA) are the current contributors of GEONETcast. The World Meteorological Organization (WMO) and other several third parties are also GEONETcast partners contributing their weather-related data dissemination.

GEONETcast also incorporates the exchange of the data between the various centers through communication satellite. This exchanging and transmission of data is received using a digital video broadcasting technology without the requirement of internet connection. The receiving station is simply satellite television dish and computer cards. This worldwide dissemination of environmental information is helping people and policy makers anywhere in the planet to import diverse information in near real time that make them informed before different natural hazards like drought are occurring (Maathuis et al., 2010).

1.2. Research Problems

In Ethiopia drought is a frequently occurring phenomenon. It is the single most important climate related natural hazard impacting on the country from time to time. About a century ago, the frequency of drought occurrence in the country was once every 10 years (Gebrehiwot et al., 2011). However, the spatial extent and frequency of drought events have both increased and it is now occurring once every five years or even less at different intensities causing significant impacts on agricultural outputs, economic losses and adverse social consequences (Gebrehiwot et al., 2011). As a consequence Farmers in Ethiopia remain highly susceptible to the recurrence of drought risks.

In order to reduce the negative impacts of drought, developing drought assessment strategies including forecasting and early warning systems is indispensable. Against this back drop, the Ethiopian government (Disaster Risk Management Unit) of the Ministry Of Agriculture and the National Meteorological Agency (NMA) are working, with support of the UN World Food Program (UN-WFP), to set up a spatial early warning assessment services for water, food supply security, as well as weather risk insurance by using different assessing tools. In Ethiopia, LEAP is the main spatial assessment tool currently applied to assess drought monitoring and early warning, by estimating Water Requirement Satisfaction Index (WRSI).

Despite the fact that LEAP has been implemented for so long as a tool for assessing drought and early warning, it has some drawbacks. Mainly, LEAP standard output indices lacks temporal and spatial details as it is dependent on a data collected from weather stations, which are generally inadequate and are sparsely located far from each other. This limits the possibilities in identifying drought proneness across the spatial units, and thereby affects the reliability of the drought monitoring tool. In addition, continuous real time information is difficult to obtain in a timely fashion as infrastructural networks are very low.

Moreover, reviews of literature reveal that there are existing limitations associated with estimating Actual Evapotranspiration (AET). On the one hand, applications of coarser resolution precipitation data for water balance model produces incomparable estimations of seasonal AET values. On the other hand surface energy balance is affected by cloud cover and sparse meteorological data, which in turn provides discontinuous estimates of AET values (Senay, 2008b). Despite those limitations, this has attracted little

scientific attention and no attempts have been made to systematically investigate both problems in a comprehensive way. Thus, a great deal of probing investigation is indispensable to support public policy and action to mitigate drought risks. Accordingly, this study attempts to fill this gap and contribute to the efforts at developing accurate drought monitoring tool in the worst affected part of the northern Ethiopia.

1.3. Research Objectives

The general objective of this research is to evaluate and compare the soil water balance and surface energy balance methodologies to estimate the water requirement satisfaction index for drought early warning assessment.

1.3.1. Specific Objectives

The specific objectives are:

- ❖ To estimate evapotranspiration from water balance approach
 - ✓ To validate TAMSAT rainfall estimates with in-situ NMA rainfall data.
 - ✓ To estimate reference evapotranspiration (ET₀) by applying FAO's penman- Monteith equation.
 - ✓ To estimate crop water requirement (ET_c) using crop coefficient (K_c) approach.
- ❖ To estimate evapotranspiration from energy balance approach
 - ✓ To estimate actual evapotranspiration (AET) with surface energy balance using GEONETcast.
 - ✓ To compare SEBS AET with GEONETcast derived land surface analysis satellite application facility (LSA SAF) AET.
- ❖ To compare WRSI result derived from soil water balance and surface energy balance

1.4. Research Questions

- ✓ To what extent is the accuracy of actual evapotranspiration derived from GEONETcast sufficient for monitoring localized drought early warning?
- ✓ How accurate is WRSI derived from GEONETcast and in- situ data streams identify localized drought trend in Tigray region?
- ✓ How comparable are WRSI estimates using soil water balance and surface energy balance model in terms of spatial distribution?

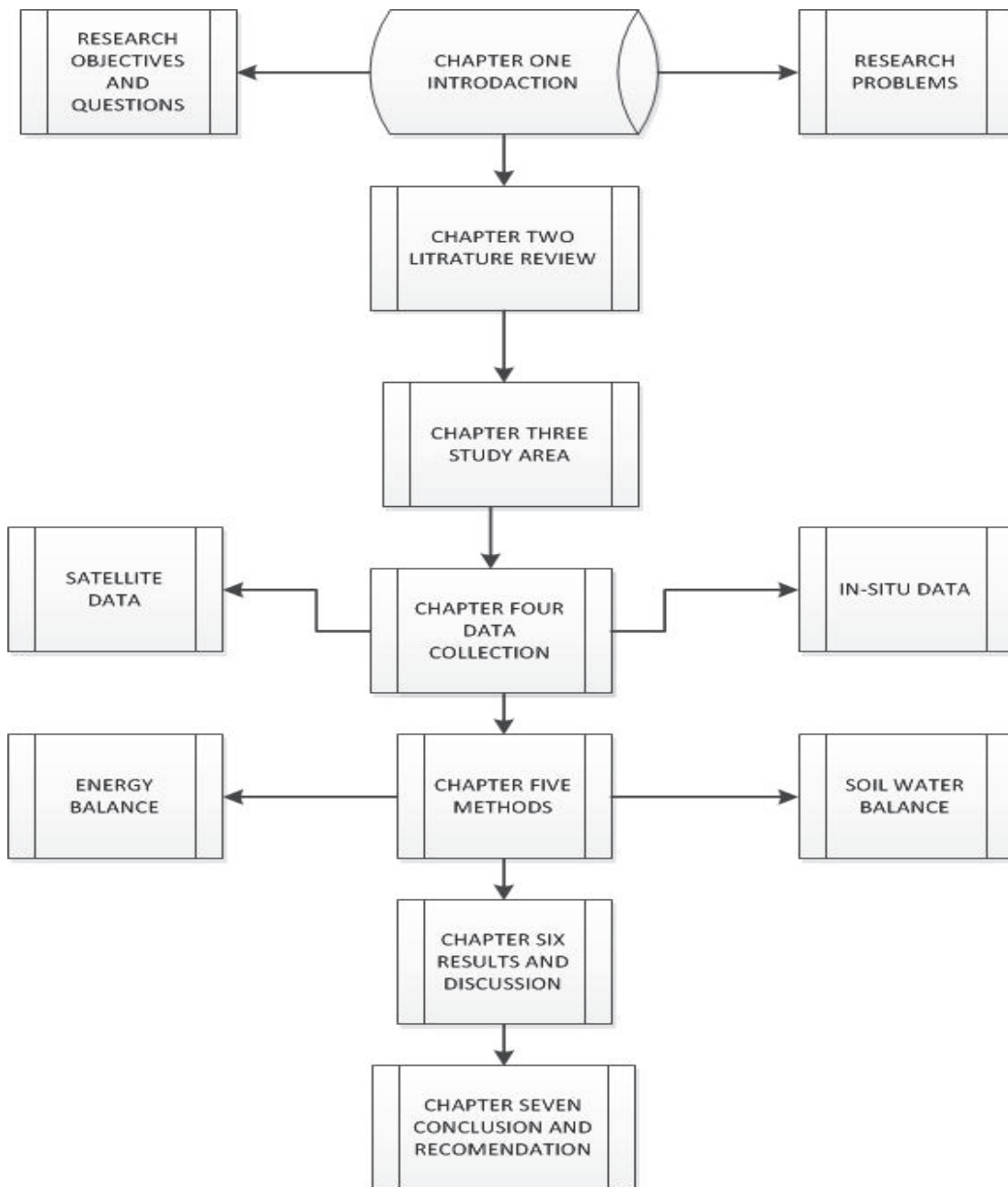


Figure 1-1: General structure of the thesis

2. LITERATURE REVIEW

2.1. Drought

Drought is usually defined both conceptually and operationally (Heim, 2002). While conceptual definition of drought is important to establish drought policy and to declare exceptional drought based on science-driven assessments, the operational definitions help to define the onset, severity, and end of droughts. This operational definition helps policy makers, resource planners, and others in recognizing and planning for drought.

2.1.1. Types of drought

- Drought can be categorized as agricultural, hydrological, meteorological, and socioeconomic droughts (Wilhite & Glantz, 1985). The first three deal with mechanisms of measuring drought as a physical phenomenon, while the last deals with drought in terms of supply and demand following the effect of shortage of rain fall.
- **Meteorological drought.** Meteorological drought is often used to compare the actual precipitation with some average or normal amount. It is considered as regionally precise since the high atmospheric conditions that result to deficiency of rainfall are highly variable from place to place.
- **Agricultural drought.** Agricultural drought is defined on the basis of deficiency of top soil moisture and susceptibility of crop during different stage of development. It links some characteristics of meteorological and hydrological drought which have agricultural impacts, giving more focus to precipitation shortages, differences between actual and crop evapotranspiration, soil water deficits, and others.
- **Hydrological drought.** Hydrological drought is often associated with the effects of precipitation deficit for surface and subsurface water supply. Like the other droughts hydrological drought also originate with a deficiency of precipitation, but this is more concerned with how the deficiency plays out through the hydrologic system.
- **Socioeconomic drought.** A socioeconomic definition of drought is associated with the vulnerability of the society due to shortage of supply of some economic good. The occurrence of socioeconomic drought depends on the time and space processes when the demand of economic goods exceeds the supply as a result of weather related deficiency of water supply.

2.1.2. Drought in Ethiopia

Drought occurs equally severe in all parts of the world (Glantz, 2001). However, its impact is higher when it occurs in developing countries especially Africa. This is attributed the fact that majority of the population depend on rain fed agriculture. Ethiopia is one of the African countries frequently exposed to extreme drought and famine throughout the human history (Gebrehiwot et al., 2011). In Ethiopia, weather risks are major determinants for occurrence of drought. Historical records reveal that there were about 30 major drought events facing the country in the past nine centuries. 13 of these drought events are known to have covered the entire nation caused severe economic losses and destroyed crops contributed to death of people and animals.

In Ethiopia, ENSO and IOD are the main causes of drought (Behera et al., 2005). The distribution of rainfall is affected by displacing and weakening of the rain-producing air masses resulted from ENSO, IOD events, and SST anomalies (Haile, 1988). The remarkable relation between Ethiopian annual rainfall and those events is due to atmospheric connection over great distance of seemingly disconnected weather

anomalies (Glantz, 2001). The oceanic and atmospheric effects in another part of the world have an effect on Ethiopian climate.

2.1.3. Drought Indices

Monitoring and analysis of drought is based on a given thresholds for forecasting precipitation deficit over a specified period of time. Different climate based drought and vegetation indices are available. (Gebrehiwot et al., 2011) some of them are Standardized Precipitation Index (SPI), Palmer Drought Severity Index (PDSI), Palmer Hydrological Drought Index, percent of normal, Crop Moisture Index (CMI), Reclamation Drought Index (RDI), Water Requirement Satisfaction Index (WRSI).

Most of the drought indices depend on accuracy and spatial extent of precipitation as the main factor in the drought calculation (Mishra & Singh, 2010). Agricultural drought generally considers availability of soil moisture in the root zone more than the precipitation deficit and the water holding capacity of the soil is the most dominant factor for occurrence of agricultural drought.

- The Standard Precipitation Index (SPI) is used to quantify the deficiency of precipitation at different time scales from shorter to longer time scales. The Short-term SPI is usually used to detect agricultural drought, while the long-term SPI is used for water supply management. SPI value ranges from -2 up to 2 in which the value 2 and -2 indicates extremely wet and extremely dry events respectively. This type of drought index is used to provide early warning for drought severity especially for shorter periods.
- Palmer drought severity index (PDSI) identifies agricultural drought based on the historical aspects of current conditions. This type of drought index can be calculated using precipitation, temperature and soil moisture and is applicable for a specific time scale of 9 months.
- Percent of normal this is used to identify the frequency of departure of precipitation from the normal and is more effective for specific region or season. It is determined by dividing actual precipitation by normal precipitation.
- Palmer hydrological drought index (PHDI) is derived from the palmer drought severity index to quantify the long-term impacts of hydrological drought. PHDI is used to determine the precipitation needed for termination of drought.
- Crop moisture index (CMI) is derived from PDSI for the effective detection of short-term agricultural drought and for crop condition monitoring.
- Reclamation drought index (RDI) combines functions of supply, demand and duration to evaluate drought reclamation plan and to release drought emergency funds.

2.2. Water Requirement Satisfaction Index

The Water requirement satisfaction index (WRSI) is an operational monitoring index, which indicates the performance of a crop based on the availability of water during growing season (Allen et al., 1998). It is determined as the ratio of seasonal actual crop Evapotranspiration (AET) to the crop water requirement (WR), which is the product of reference crop evapotranspiration (ET₀) and crop coefficient (K_c) value of the specific crop (Senay et al., 2011). AET represents the actual amount of water withdrawn from the soil water reservoir and can be estimated by energy balance and water balance methods. WRSI acts as a tool to evaluate the crop water status in the next decade based on the availability of moisture in the soil. Quantitatively it can be represented as percentage and it has four broad categories.

- i. An index between 80-100% indicates sufficient water in the root zone to support the crop without water stress for the next decade.
- ii. 70 – 79% indicates there is satisfactory water in the root zone and this shows conditions ranging from smaller degree of water stress to sufficient soil moisture.
- iii. 50 – 69%, is an indication that the crop is likely to experience from severe to moderate water stress
- iv. finally is the index value of 0 – 50% and this indicates the soil is already at very low moisture level which can cause permanent wilting point and crop failure (Senay, 2008b).

WRSI model requires a start-of-season (SOS) and end-of-season (EOS) time. The threshold used to determine SOS is based on the amount and distribution of rainfall received in three consecutive decades. On the other hand, the end of seasons (EOS) is estimated by adding Length of Growing period (LGP) and SOS. The determined WRSI value of a given pixel represents the seasonal integrated conditions from the start of the growing season until the time of modelling (Brown, 2008).

2.3. Water Balance Concept

The availability of water in the root zone is important to support plant growth and crop production. Rain water or irrigation reaching an area of soil surface, experiences different processes some infiltrate into the soil and some leave the area as surface runoff. The infiltrated water also may evaporate directly from the soil surface to the atmosphere, consumed by plant roots for growth and transpiration, accumulate within the root zone or it may percolate downward beyond the root zone. When rainfall amount or the irrigation water is not sufficient, the soil moisture content in the root zone is reduced to levels that can't tolerate the crop water requirement ET_c . This results in less actual evapotranspiration than the ET_c , and the plants experience water stress.

Actual evapotranspiration is generally a fraction of ET_c depending on soil moisture availability. Most of the time Actual evapotranspiration approaches ET_c during the active growing stage of crop, when sufficient amount of moisture is available in the soil. However, it falls below ET_c during early growth stage, prior to full canopy coverage, and the end crop growing stage. As a result, rain-fed crops which cover more than 80% of the global cropped area and 60–70% of global crop production is frequently limited by soil moisture stress (Biggs et al., 2008).

2.4. Evapotranspiration Concepts

ET is a process which governs the water cycle and energy transport between the soil-water-vegetation system and the atmosphere (Senay, 2008a). It combines two separate simultaneously occurring processes evaporation and transpiration. Evaporation occurs on the surface of open water bodies, vegetation and bare ground whereas transpiration transports water from the soil through the plant roots from the leaf (Senay et al., 2011). Global warming, natural hazards and species extinctions causing global environmental changes are the main concern of all today. ET which governs those processes plays an important role in hydrology and agriculture for prediction and estimation of global climate change.

The spatial distribution and accurate quantification of evapotranspiration is important to determine crop water stress. Understanding the rate and amount of evapotranspiration is essential for monitoring hydrological and agricultural systems (Elhag et al., 2011). Because of its important role in hydrology, meteorology and agriculture it is advisable to have reliable information of ET to predict natural hazards such as drought.

Radiation, air temperature and crop characteristics are weather parameters affecting evapotranspiration. Although it is not possible to measure ET directly, there are convectional ET estimation techniques (i.e., pan-measurement, Bowen ratio, eddy correlation system, and weighing lysimeter). Convectional techniques are based on field measurements and provide better estimation of ET over a homogeneous area (Li et al., 2009). Most of these techniques require surface and land parameters which are difficult to obtain over large-scale areas, and this in turn limits its applicability. However, remote sensing base estimates of ET provide consistent and economic feasibility on regional scales (Ayse, 2008). Besides, it provides continuous spatial information within a short period of time and practically useful especially for ungauged areas.

2.4.1. The Surface Energy Balance System

The surface energy balance system (SEBS) was developed to estimate atmospheric turbulent fluxes at different land surface physical properties using satellite data (Su, 1999). Surface energy balance governs the exchange of water and partitioning of the surface turbulent fluxes into sensible and latent heat fluxes in the soil-vegetation-atmosphere interaction. According to Su (2002), SEBS requires the following three input data sets to derive evapotranspiration flux per pixel.

- i. Remotely sensed land surface parameters which include: albedo, emissivity, LST, FVC, and LAI.
- ii. Meteorological parameters that include air temperature and pressure, wind speed and relative humidity.
- iii. Radiation data: downward short wave and long wave radiation.

The SEBS model is a single energy balance model capable of providing accurate estimates of AET which is critically important for drought assessment based on the general surface energy balance equation.

2.5. Concept of GEONETcast

The use of earth observation data for different purposes mainly in the developing world still remains unexploited, though there is an increasing earth observation (EO) data delivery (Mannaerts et al., 2009). Consequently, lack of reliable and continuously accessible real time environmental information was frequently exposing these countries to serious environmental problems. Currently, GEONETcast tool is providing a conducive environment in capacitating developing countries through enhancing information communication and providing fast, cost-effective, and efficient access to environmental information (Maathuis et al., 2010).

GEONETcast is a near real-time data dissemination system by which environmental in-situ, air and space borne products are transmitted to users through satellites. It was developed by the Global Earth Observation System of Systems (GEOSS) to alleviate the barriers for accessing and use of EO data. This allows users anywhere in the world to access Earth observation data without limit (Maathuis et al., 2010). This low cost, global, environmental information delivery system is currently operating in the whole world to ensure data stream transmitted through communication satellites can be received using simple and cheap ground reception infrastructure (Figure 2.1). This contains low cost digital satellite television data reception and computer based storage system. Meteosat image data, GOES East and West image data, EUMETSAT meteorological products, NOAA-NESDIS meteorological products, CMA FY2C satellite images and meteorological products are the available GEONETcast products and services.

The Meteosat Second Generation satellites established by European Space Agency (ESA) and European Organization for the Exploitation of Meteorological Satellites (EUMETSAT) is the main satellite used in the GEONETcast. Different satellite datasets of MSG are used in developing world especially in Africa from GEONETcast (Ataklti, 2012; Gelassie, 2012).

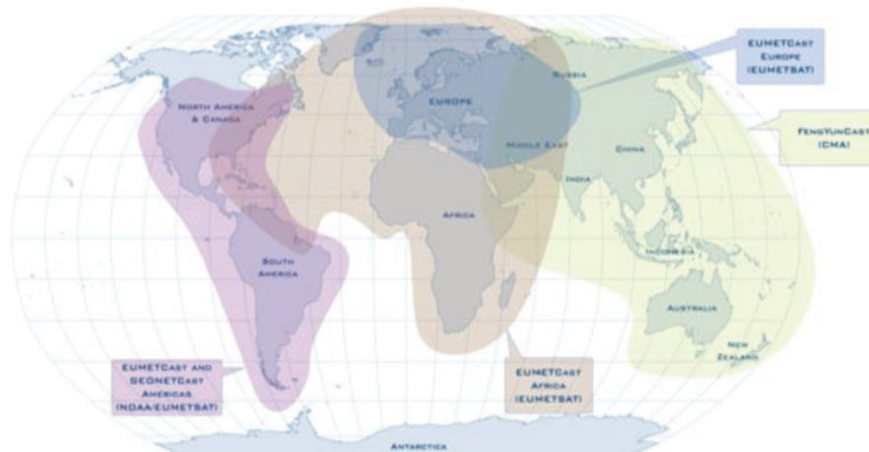


Figure 2-1:-GEONETcast global coverage

3. STUDY AREA

3.1. Location and administration divisions

Location

The study area, Tigray, is one of the national regional states of Ethiopia. Geographically Tigray is located in the Northern part Ethiopia between latitudes 12°15'N and 14°57'N and longitudes 36°27'E and 39°59'E covering a total area of 53,000 square kilometres (Gebrehiwot et al., 2011). The region is bordered with Eritrea to the North, the Sudan to the West, and with Ethiopian regions of Amhara and Afar to the South and the East respectively. The state is divided into seven administrative zones including the capital Mekelle, 13 urban districts and 34 rural districts (locally called *woreda*- the second administrative level below the zone) and is autonomous to manage its overall activity.

The region has a total population of over 4.3 million with an average family size of five persons per household (CSA, 2008). According to the 2007 housing and population census, the population is growing at a rate of 2.5 per cent per year and population density in the region is 86.6 persons per square kilometre, showing a high population pressure. Regarding ethnic group composition, 97.58 per cent of the population is *Tigray*, 0.7 per cent *Erob*, and 0.07 per cent *Kunama*. Tigrigna is the working language in the region.

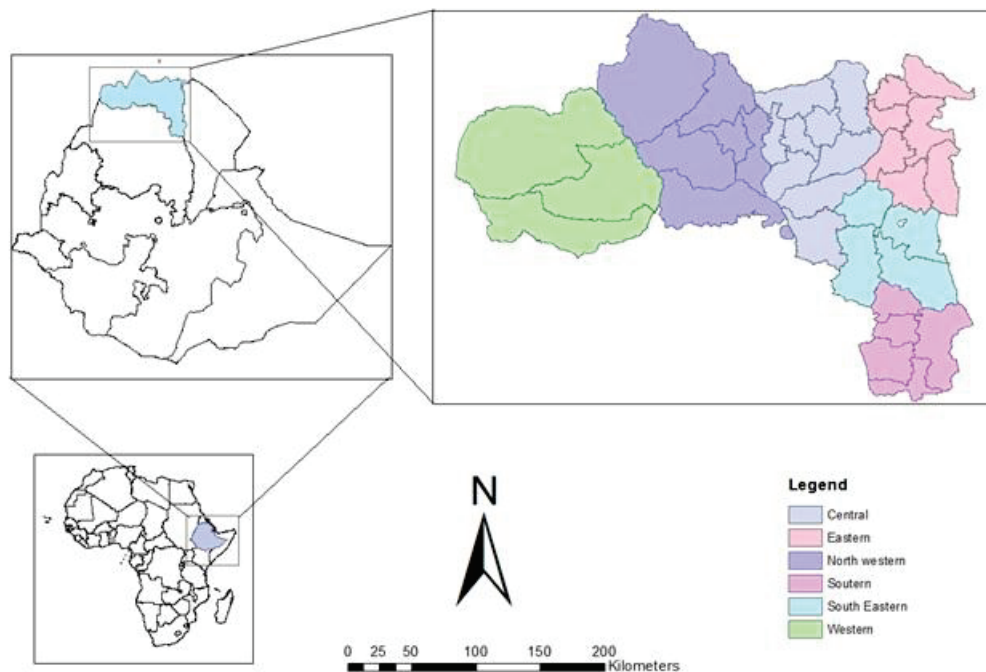


Figure 3-1:-Location Map of the study area

3.2. Agro-ecological zonation

Presence of complex topography is one of the major factors for the existence of a variety of environmental features in Ethiopia. Despite the complexity of the topography it has generally become a common practice to classify the country into lowland areas (< 1500 meters above sea level) and highland areas (>1500 meters a.s.l.). Similarly, Tigray has a diverse topography, with an altitude that varies from about 500 meters above sea level in the northeast to almost 4000 meters a.s.l in the southwest as shown in fig.3.2. About 53 % of the land is lowland (*kola* – less than 1500 meters a.s.l.), 39 % is medium highland (*weina-degua* – 1500 to 2300 meters a.s.l.), and 8 % is upper highland (*Degna* – 2300 to 3000 meters a.s.l.) (Hagos et al., 1999). The wide range of altitude governs the temperature and climatic conditions of the region (Tesfay, 2006). This marked variation in altitude results in a distinct spatial distribution of temperature and rainfall.

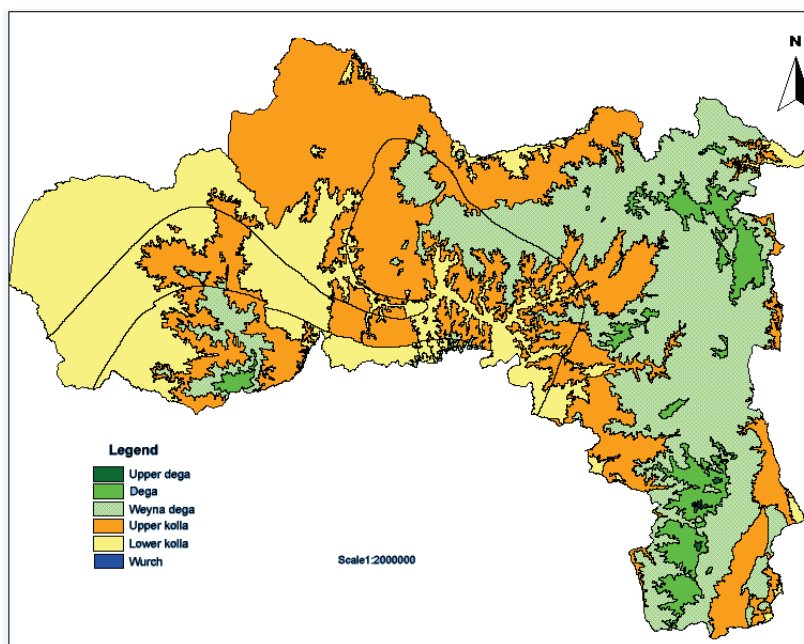


Figure 3-2:-Agro-ecological zone based on altitude, BOFED 2002

3.3. Climate

The region belongs to the sub-tropical climate which is characterized by sparse and highly uneven distribution of seasonal rainfall and frequent drought. The main rainfall season locally called *kiremti* starts in June and lasts until September. Rainfall in the region is highly variable temporally and spatially, which results in strong variation in yields of crops and livestock. Average rainfall varies from about 200 mm in the northeast lowlands to over 1000 mm in the south west highlands (Hagos et al., 1999). According to Gebrehiwot et al., (2011), the mean annual rainfall of the region is estimated to be 473 mm, 84% the annual rainfall. The average annual temperature varies from <7.5 °C in locations >3500 m a.s.l. to > 27 °C in the eastern lowlands.

3.4. Landuse and Landcover

Given the ages of human occupation, little remains of the original vegetation cover in the northern Highlands. The current land cover comprises a mosaic of cultivation, with grassland and shrub land. In the Lowlands there remains an extensive area of woodland and shrub land with areas of shifting cultivation. The major land use forms are grazing, cultivation, forests and woodlands. More than 50 % of

Ethiopia's land is utilised for grazing (of which 36.2% bush and shrub land and 22.78% are grass lands). Cultivation forms the second largest (nearly 28.21%) land use while other forms of land use account for 10.8 % of the land mass (Pender et al., 2004). The natural forest resource of the region is extensively exploited and accounts only about 0.2 % of the total land area. The decline in forest cover has a long history and is closely linked with human economic activities and population pressure (Nyssen et al., 2004). In Tigray, agricultural land use expansion is increasing at the expense of maintaining natural vegetation in the region and this resulted to the frequent occurrence of drought (Nyssen et al., 2009). The land cover map of Tigray region classified from the European Space Agency (ESA) Global Land Cover map with spatial resolution of 300m for the year 2009 is depicted in Fig.3-3.

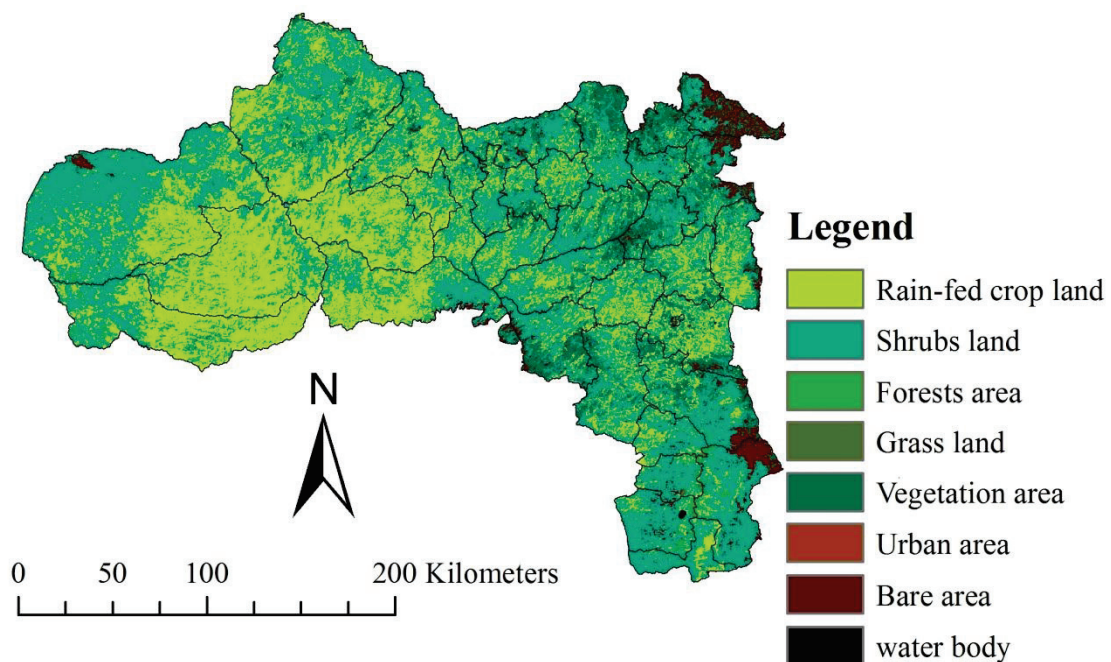


Figure 3-3:- Land cover map of Tigray

3.5. Drought Situation

Like the rest of Ethiopia, the economy of Tigray is heavily dependent on low productivity rain-fed agriculture that strongly dependent on timely onset amount and distribution of rainfall (Araya & Stroosnijder, 2011). Agriculture is the main source of economy for the majority of the population. It covers about 52.9 % of GDP. Crop husbandry, animal husbandry and mixed farming are the main farming systems, of which mixed farming is the dominant type of farming system. Smallholder farmers manage crop and animal production in an integrated way, to maximize returns from their limited land and capital, minimize production risk, diversify sources of income, provide food security and increase productivity.

Smallholder agriculture predominates with an average land holding of less than one hectare per family. Agricultural systems in the region are characterized by traditional technology based entirely on animal pull and rain-fed agriculture. Almost all of the cropland is planted to annual food crops, including cereals (teff, wheat, barley, maize, sorghum, millet), pulses (beans, chick peas, lentils), and oilseeds (sesame, flax).

Agricultural productivity in the region is low, even when compared with the national average. The average regional yield is 0.8 tons/ha (BOFED, 2004). Poor soil fertility, highly erratic rainfall, and limited use of modern inputs are among the factors that contribute to the low level of agricultural productivity in the region.

Tigray is one of the regions repeatedly affected by repeated cycle of drought and food security problems in the country. Poverty and food insecurity are highest in the highlands of Ethiopia (Diao, 2010). Populations engaged in agriculture are particularly at risk from drought as agriculture is the major climate-sensitive economic activity.

Drought is a major frequently occurring hazard affecting crop and livestock production in most parts of Tigray. The frequency, intensity; amount and duration of rainfall play critical roles in the occurrence of drought (Gebrehiwot et al., 2011). Over the year's farmers experience the worst effect of drought in terms of their loss of crop yield and livestock, and sometimes crop failure due to scarcity of water during peak growth stages of the crop. The magnitude of this is well understood from the fact that the region is an agricultural region with 82 % of the population directly depend on agriculture for their livelihood. Owing to the abnormalities in terms both spatial and temporal distribution of precipitation, drought is a frequent phenomenon which cause instability in food production over many parts of the region (Araya & Stroosnijder, 2011).

4. DATA COLLECTION

In this research different datasets were used:

- ✓ Ground observation data
- ✓ Crop specific data
- ✓ Meteorological data
- ✓ Remote sensing Data

The different datasets useful for this research are summarized in table 4-1

Table 4-1:-Description of different data sets used in this study

Data set	Variable	Description	Resolution	
			Temporal	spatial
TAMSAT	Rainfall	Satellite	decadal	4km
Land SAF AET,	AET	Satellite	30 min	3km
albedo, LST, DSSF, DSLF, NDVI,LAI,FVC	Land surface parameters	Satellite	15 min to daily	3km
Meteorological data	Rainfall, max. & min. temp. wind speed, sunshine hours, humidity	Ground station	Point	Point
ECMWF	Meteorological data	satellite	From 3hr to daily	0.75°
SPOT vegetation	Land cover	satellite	decadal	1km

4.1. Ground observation data

4.1.1. IN-situ Data

Field work was conducted in Ethiopia from September 6 to October 7, 2012. During the field work different data was collected from different organisations such as the national meteorological agency of Ethiopia Tigray branch, Tigray bureau of agriculture and rural development. In addition, field campaign that includes interview with local farmers and land cover validation was conducted in different weredas (districts) in the region. The land cover validation was conducted randomly in districts of Wukro, Adigrat, Adwa and Adigudom.

4.1.2. Land Cover Data

Information of land cover was collected using ground positioning system (GPS) and digital camera. These data are required to understand the crop condition, to identify the major crops growing in the regions and to observe the rain fed agricultural crops for validation of the surface energy balance model products.

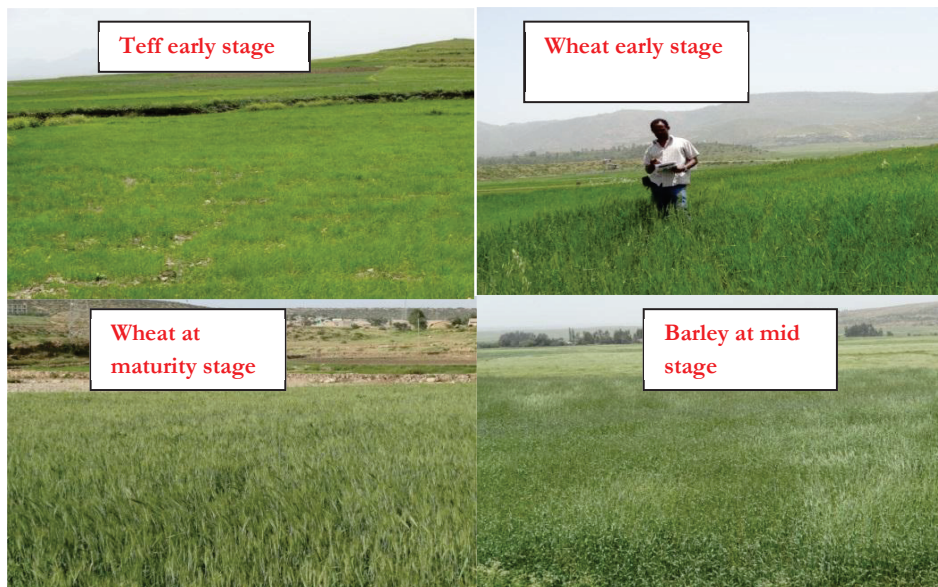


Figure 4-1:-Major rain fed crops growing in the study area

4.2. Crop specific data

4.2.1. Crop Coefficient and Crop Calendar

The crop coefficients (K_c) used for this study were obtained from the LEAP software. In this tool the K_c values of 15 major crops of the country are listed. From those, K_c values for the three major crops growing in the area (barley, Teff and wheat) were selected and are given in table (5.1). The other parameter required for this research is the crop calendar. The crop calendar used during this study for the major crops growing in the region were taken from United States Department of Agriculture (USDA) that shows the crop calendar for the whole country. Furthermore this crop calendar was enhanced by field campaign.

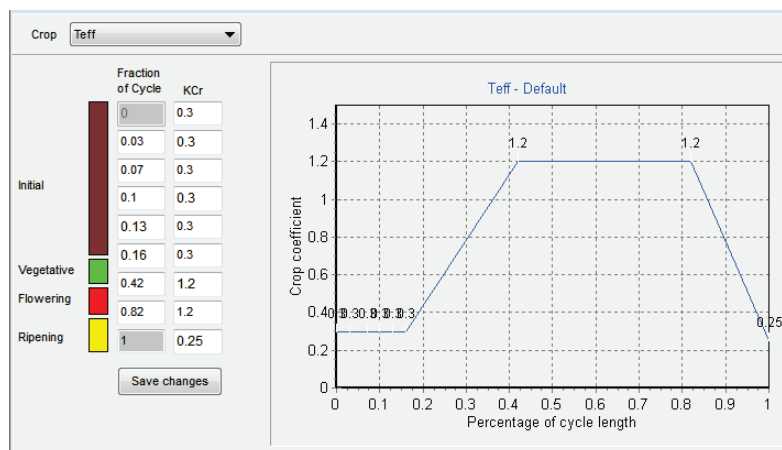


Figure 4-2:- K_c values for the major crops in the area taken from LEAP

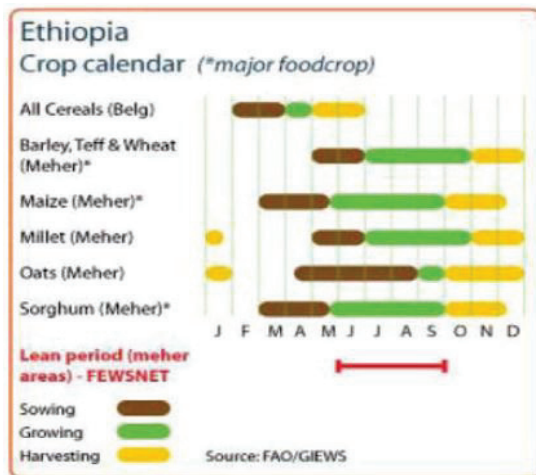


Figure 4-3:-Ethiopian major food crop calendar

4.3. Meteorological Data

Determination of reference evapotranspiration using Penman-Monteith and the surface energy balance model requires meteorological data products like vapour pressure, maximum and minimum temperature, air pressure, relative humidity, wind speed at reference height, and sun shine hours. Those were collected from National Meteorological Agency (NMA) Tigray branch synoptic or class A weather stations while additional rainfall data were collected from class 4 weather stations. The weather stations were selected because they contain representative data sets for this research and considerably represent the study area. The meteorological datasets collected from Tigray synoptic and class 4 weather stations are on daily basis for the period 1st January 2008 to 30th of September 2012. Although the analysis was conducted for 2012 main growing seasons from 1st may to 30th September 2012, the other data products were used to fill missing data.

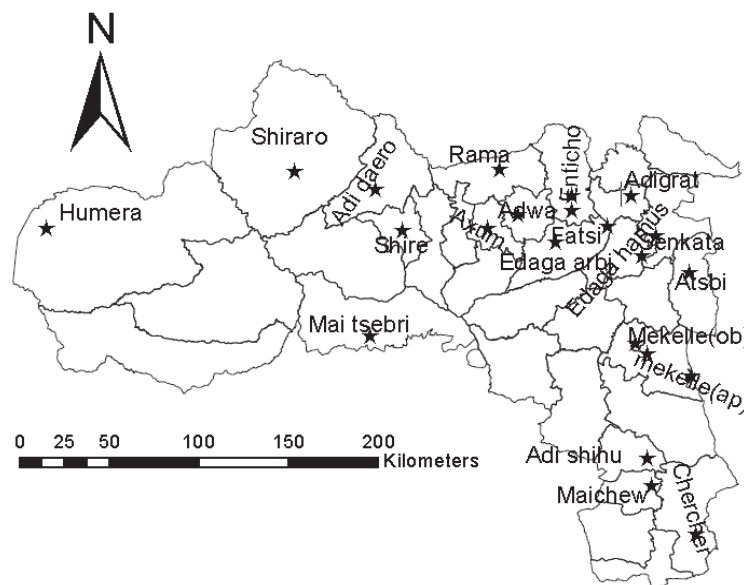


Figure 4-4:-Total weather stations available in the study area

Table 4-2:-Currently Working Synoptic Meteorological stations

Station	Lat	Lon	Started Year
Adigrat	14.28	39.45	1970
Adwa	14.18	38.88	1953
Atsbi	13.88	39.74	N/A
Axum(A/port)	14.14	38.78	N/A
Chercher	12.54	39.77	N/A
Fireweini	14.07	39.57	2000
Humera (Old)	14.10	36.52	1968
Humera(airport)	14.10	36.52	1972
Maichew	12.79	39.55	1976
Maytsebry	13.56	38.14	2005
Mekelle (AP)	13.47	39.53	1959
Mekelle (obs)	13.52	39.47	1973
Shiraro	14.40	37.76	2002
Shire Endasilasse	14.10	38.30	1973
Tekeze Hydro power	13.36	38.77	N/A

Note: N/A stands for not available (the year of establishment is not known)

4.3.1. European Centre for Medium-Range Weather Forecasts

The European Centre for Medium-Range Weather Forecasts (ECMWF) centered in Reading, England is an independent intergovernmental organization supported by European Member States and other Co-operating States to provide accurate medium-range, monthly and seasonal worldwide weather forecasts (Simmons et al., 2007). ECMWF provides a wide range of forecast for Meteorological and oceanographic products to the general public and enhanced products to member States and other registered users. Parameters such as boundary layer height, mean sea level pressure, surface pressure, air temperature at 2m, 2m dew point temperature, sunshine duration and 10m U & V wind components were required for this study. Those products were downloaded free of charge from 1st May 2012 to 30 September 2012 at a spatial resolution 0.75 degree (around 83 km.) and temporal resolution of 6 hours to daily from ECMWF website (http://dataportal.ecmwf.int/data/d/interim_full_daily)

4.4. Satellite Data

The Spinning Enhanced Visible and Infrared Imager (SEVIRI) on board of meteosat second generation MSG provide imagery data using 12 spectral channels at the European Organization for the Exploitation of Meteorological Satellites EUMETSAT facilities in Darmstadt, Germany (Trigo et al., 2011). Those additional channels available on MSG satellite provide a wider range of spectral information.

EUMETSAT was established for sustainable exploitation of meteorological satellites and is providing imagery data from different satellites. In the house of EUMETSAT the received imagery data from MSG are processed and broadcasted to the users around the globe. This transmits satellite and in situ data products and services from the Global Earth Observation System of Systems (GEOSS) using satellite communications. It is also accountable for the operation and monitoring of the EUMETCast GEONETcast data dissemination system through satellite. This includes transmission and monitoring of transmitted product for proper data reception to give access to the user free of charge.

The main EUMETCast GEONETcast satellite data products used for this study are

- ✓ Tropical Applications of Meteorology using Satellites (TAMSAT) data
- ✓ Satellite Application Facility for Land Surface Analysis (Land-SAF) data

4.4.1. Tropical Applications of Meteorology using Satellites

TAMSAT is the product of seasonal rainfall estimates RFE for Africa derived from Meteosat thermal infra-red (TIR) channels based on the recognition of convective storm clouds (Thorne et al., 2001) and calibration against ground-based rain gauge data. The product is delivered to the user in decadal ten days and monthly temporal resolution and spatial resolution of 4km. Rainfall Estimates for periods of a week or more can be mainly used to identify periods of low rainfall which can lead to crop failure, while those estimated at a daily or shorter are used for flood forecasting and river management (Beyene & Meissner, 2010). Due to this reason the decadal resolution was selected for this study and it was downloaded from the GEONETcast tool box from 1st May to 30th September 2012.

4.4.2. Satellite Application Facility for Land Surface Analysis

The Satellite Application Facility for Land Surface Analysis (Land-SAF) is part of the SAF network, a set of specialized development and processing center EUMETSAT. Its main purpose is to take full advantage of remotely sensed data from EUMETSAT sensors, to measure land surface variables.

The Land-SAF makes use of MSG, and the EUMETSAT Polar System (EPS) satellites to provide more timely information and these were especially designed to serve the needs of numerical Weather Prediction (NWP). The products retrieved from LSA SAF include down waling long (DSLRF) and shortwave (DSSF) surface fluxes, albedo (AL), land surface temperature (LST), emissivity (EM) leaf area index (LAI) fraction of vegetation cover (FVC) and actual evapotranspiration (AET) with temporal resolution of 15 min to daily and spatial resolutions of 3km. In this research, all the LSA SAF products were downloaded from the LSASAF dissemination center available on (<https://landsaf.meteo.pt>) from 1st May to 30th September 2012.

5. METHODS

WRSI for the three major crops in the area can be estimated based on the water supply and the requirement of the crops during a growing season. This was calculated as the ratio of actual evapotranspiration AET to seasonal crop water requirement WR as shown below.

$$WRSI = \frac{AET}{ETc} * 100$$

1

where AET is the actual evapotranspiration [mm day⁻¹]

ETc is the is the water use pattern of a crop [mm day⁻¹]

The ETc was calculated from the FAO reference evapotranspiration that is adjusted with appropriate crop coefficient (K_c) value. The calculation of this WR is explained in more detail in section 5.1.

The actual evapotranspiration AET was estimated in two approaches, as mentioned in figure 5-1.

1. Using soil water balance method which requires meteorological data, satellite rainfall data, crop properties and soil properties. This is explained in more detail in paragraph 5.2.
2. Using surface energy balance method that uses satellite, meteorological and other model output data sources. This is explained in more detail in paragraph 5.4.

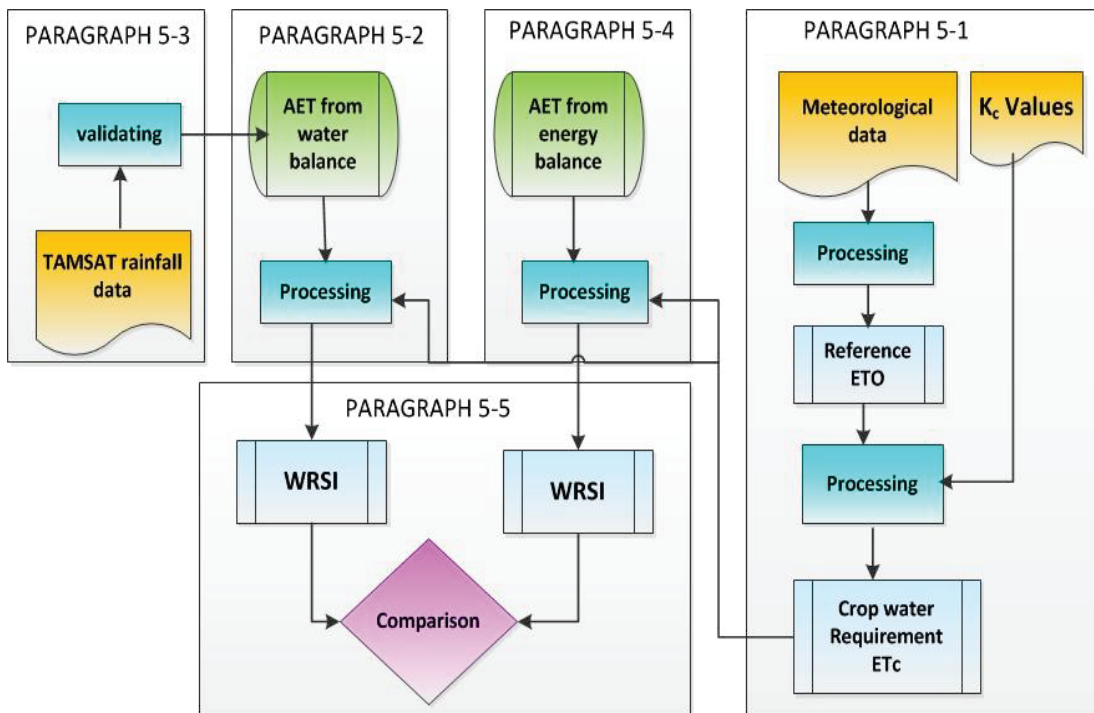


Figure 5-1:-WRSI flow chart

5.1. Estimation of Crop Water Requirement

Crop water requirement characterizes the evapotranspiration from disease-free, well-fertilized crops grown in optimum soil water conditions (Allen et al., 1998). It differs from the reference evapotranspiration (ET₀) in its ground coverage, canopy properties and aerodynamic resistance of the crop. There are different ways of determining evapotranspiration: direct measurement, indirect methods (from weather data and soil water balance) empirical methods and physical based methods in which they vary in terms of data requirement and accuracy (Allen et al., 2005b).

In this study the crop water requirement was calculated using the crop coefficient approach. In this approach most of the weather condition effects are incorporated in the estimation of reference evapotranspiration ET₀ while the specific crop characteristics like canopy resistance, crop height and reflectance of the crop soil surface are predominantly characterized by the K_c value that vary according to the growing season of the specific crop (Araya et al., 2011).

Based on Allen et al. (2005a), the growing stage of the major crop in the area was divided in to 4 stages as initial stage which starts from the planting date to approximately 10% ground cover, development stage starting from 10% ground cover to effective full cover, mid-season stage this runs from effective full cover to the start of maturity and finally the late season stage that starts from the start of maturity to the harvest (FAO, 2007). The ET_c for the three major crops growing in the study area was estimated on decadal basis using the single K_c approach. During the calculation the K_c values in the initial and mid-season stages were considered constant while that of developing and late season stages were changing every decade (Allen et al., 2005a).

ET_c was calculated simply by multiplying the reference evapotranspiration with crop coefficient values.

$$ET_c = K_c * ET_0 \quad 2$$

where, ET₀ –is the reference evapotranspiration [mm d⁻¹]

K_c –crop coefficient [-]

The numerical representation of K_c value at any period in the growing season of the crop were estimated by

$$K_{ci} = K_{cprev} + \left(\frac{i - \sum(L_{prev})}{L_{stage}} \right) (K_{cnext} - K_{cprev}) \quad 3$$

where i – length of growing season (day)

K_{ci} crop coefficient on day i

L_{stage} length of the stage under consideration (day)

$\sum L_{prev}$ Sum of the lengths of all previous stages (day)

Table 5-1:-Kc and root depth fraction of the three major crops in the study area

Crop	Initial	Developing Stage	Mid-season Stage	End Stage	Root depth fraction	
					Initial	Developed
Barley	0.3	1.2	1.2	0.25	0.3	0.5
Teff	0.2	1.2	1.2	0.25	0.2	0.5
Wheat	0.3	1.2	1.2	0.25	0.3	0.5

5.1.1. Estimating Reference Evapotranspiration

The reference evapotranspiration (ET₀) was calculated by the FAO Penman-Monteith method. It is the evapotranspiration from a reference surface where the reference surface is a hypothetical grass which is assumed to have crop height of 0.12 m, surface resistance of 70 s m⁻¹ and an albedo of 0.23' (Allen et al., 1998). In this research the reference evapotranspiration of the study area was calculated using meteorological data collected from 13 synoptic classes "A weather stations for the period of 1st may up to 30th September 2012 on daily basis.

The general FAO Penman-Monteith equation to calculate reference ET₀ is given by

$$ET_0 = \frac{0.408 * \Delta(R_n - G) + \gamma \frac{900}{T + 273} U_z (e_s - e_a)}{\Delta + \gamma(1 + 0.34U_z)} \quad [\text{mm day}^{-1}] \quad 4$$

where, R_n is net radiation at the crop surface [MJ/m²day]

G-is soil heat flux [MJ/m²day],

T- is daily mean air temperature [°C]

U_z is wind speed at 2m height [m se⁻¹]

e_s -is saturation vapour pressure [kPa]

e_a is actual vapour pressure [kPa]

$e_s - e_a$ -is saturation vapour pressure deficit [kPa]

Δ is slope of vapour pressure curve [kPa/°C]

γ is psychometric constant [kPa/°C]

For this calculation different steps were undertaken. The collected meteorological data were pre-processed and arranged according to the requirements for the calculation of different parameters in equation (4).The detail pre-processing steps for the parameterization of Penman-Monteith equation is given in appendix A.

5.2. Estimating AET from Soil Water Balance Model

Calculating the water balance of a given study area is an important approach for determining water stored in different components of the hydrologic cycle and the water exchange between these components. In this research to calculate the soil water balance and to quantify moisture deficit, different steps were taken. Different meteorological parameters, textural soil properties and GEONETcast rainfall data products were analysed. The TAMSAT rainfall data for the study area was produced using sub map operation in ILWIS from the rainfall map covering the whole Africa. The textural classification of the soils in the study area was also analysed.

According to FAO digital soil map it is categorized under 3 major classes namely very clayey texture in the western part of the region, loamy sand texture in the eastern part and silty clay in the other part of the area. The soil water content present in the soil at any time was estimated from the water holding capacity (WHC) of the specific soil. The WHC is the amount of water available in the soil and was estimated from the difference in moisture content between field capacity and wilting point (FAO, 2007). The WHC values for each soil in the area were taken from FAO 56 paper

AET for the major crops growing in the area (Teff, wheat and barley) was estimated on decadal basis according to the following equations.

$$AET = ETc \quad \text{when } PAW \geq SWC$$

$$AET = \frac{ETc}{SWC} * PAW \quad \text{when } PAW < SWC$$

$$AET = PAW \quad \text{when } AET > PAW$$

$$SW_i = SW_{i-1} + PPT - AET \quad 5$$

where PAW - plant available water [mm]

PPT- decadal precipitation [mm]

SWC - the critical soil water level

SW_i - soil water content at the end of the ith time interval [mm/decadal]

SW_{i-1} - soil water content at the end of the previous ith time interval [mm/decadal]

PAW is the portion of total available moisture which can be extracted by plants without having water stress and was calculated by:

$$PAW = SW_{i-1} + PPT \quad 6$$

SWC is the critical soil water level below that the actual crop water requirement (AET) is less than the crop water requirement (ETC) and was parameterized with fraction of water holding capacity (SW_f) and root depth fraction (RD_f) according to the following equation.

$$SWC = WHC * SW_f * RD_f \quad 7$$

Where -SW_f is the average fraction of WHC of the soil that can be depleted from the root zone before moisture stress. It varies from 0.3 for shallow rooted plants to 0.7 for deep rooted plants or average value of 0.5 is commonly used for many crops and this value was taken for this study.

RD_f root depth fraction which is different for different crops and it also varies according the growing period of the same crop. This increases linearly from the initial to the mid-season of the growing stage.

In the estimation of AET with the water balance model the physical feature of the study area characterized by valleys and hills that facilitate soil erosion and affect the soil moisture availability, the prolonged 7-8 months of dry season before the main rainy season *Kiremti* and the deeper groundwater table were considered. Based on the above considerations the soil moisture content at the beginning of the growing season was assumed to be zero (Liu et al., 2012; Reynolds et al., 2000).

5.3. Precipitation

A quantitative evaluation of the amount and spatial distribution of precipitation is required for a number of large scale hydrological applications and for mapping rainfall patterns in a specific area. In the study area, precipitation is the primary determinant factor for crop production. However, it is highly variable in terms of duration and intensity as shown in figure (5-2) and this variability significantly affect the economy and the environment of the study area.

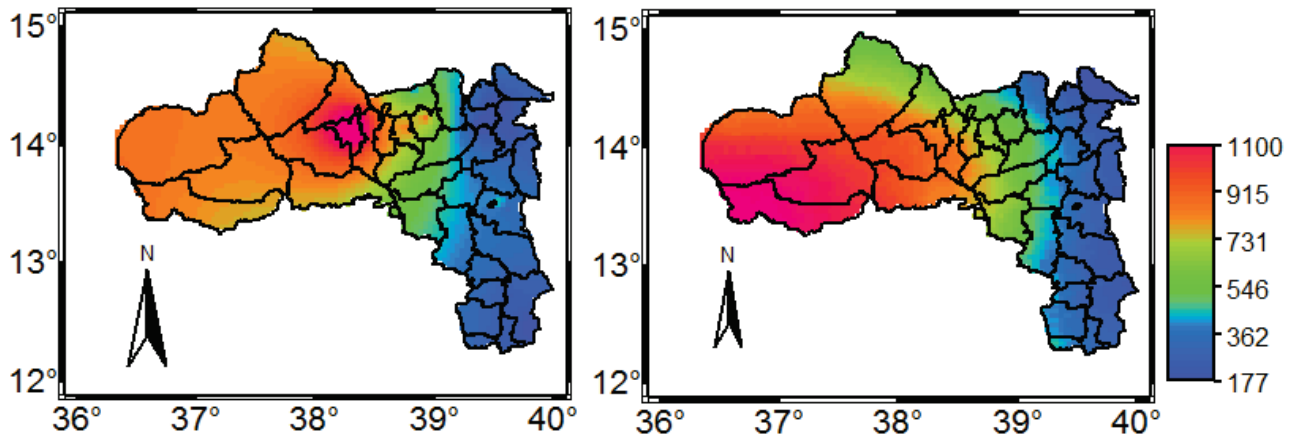


Figure 5-2:-Total in situ (left) and satellite (right) rainfall of the area for 2012 growing season

5.3.1. Reliability of Gauge Rainfall data

The study area is characterized by sparsely located weather stations and continuous rainfall records are difficult to obtain. Therefore, the reliability of the rainfall data collected from the stations was evaluated using double mass curve. The double-mass curve is used to check the consistency of hydrologic data by comparing the cumulative value for a single station with the average cumulative values from several other stations around it. Breaks in the double mass curve shows there is a change in the relation of the two variables and this change indicates the inconsistency of the records. The inconsistency may be due to data collection problems or shifting of the rain gauge to a new location due to natural climatic problems. In this research out of 19 rainfall weather stations 15 were evaluated using double mass curve technique and the quality was checked with statistical objective functions, correlation coefficient (R^2) and root-mean-square error (RMSE). The other 4 stations were not considered due to missing records. In this case those stations having RMSE of above 30mm and R^2 of below 0.5 are considered as problematic stations and are not considered for further analysis. Out of the 15 stations 2 stations show higher RMSE and were omitted from the list while 13 stations were qualified for the reliability test and were used for further validation of the satellite rainfall data.

$$RMSE = \sqrt{\sum_{i=1}^n \frac{1}{N} (s_i - G_i)^2} \quad 8$$

where, RMSE is root mean square error, S_i is satellite estimate, G_i is the ground truth and N is number of samples.

5.3.2. Comparison of TAMSAT Rainfall with In-situ Rainfall

The objective of this comparison was to investigate the accuracy of the satellite rainfall estimates and determine their advantages and limitations for parameterizing soil water balance model. Accordingly the

rainfall data from the reliable weather stations were selected for the period of 1st may 2012 to 30th September 2012. In this study pixel by pixel and point to pixel comparison of the two rainfall data was performed.

The pixel to pixel comparison was carried out after spatial interpolation of the decadal rainfall gauge data from the reliable stations using inverse distance weighting method with pixel size of 4km. Inverse distance weighted (IDW) is commonly used technique for interpolation of point data and works based on the concept that, areas that are far from the gauge should be assigned smaller weights than those that are closer in distance. Here the interpolating surface is mostly influenced by the nearby points and less by the more distant points. The interpolated decadal rain gauge data was compared to decadal satellite precipitation estimates to evaluate the areal estimation rainfall rather than point in order to calculate a number of statistical parameters on a pixel-by-pixel basis.

Finally point to pixel comparison of the rain fall was done on the reliable stations. In this case the collected daily rainfall value from the ground gauge was summed to get decadal rainfall value in order to have the same temporal resolution with the satellite. The rainfall value from the satellite was extracted using map value in ILWIS for each point that represents the stations on the ground and the comparison was performed between the rainfall values from the stations with the values extracted from TAMSAT rainfall image.

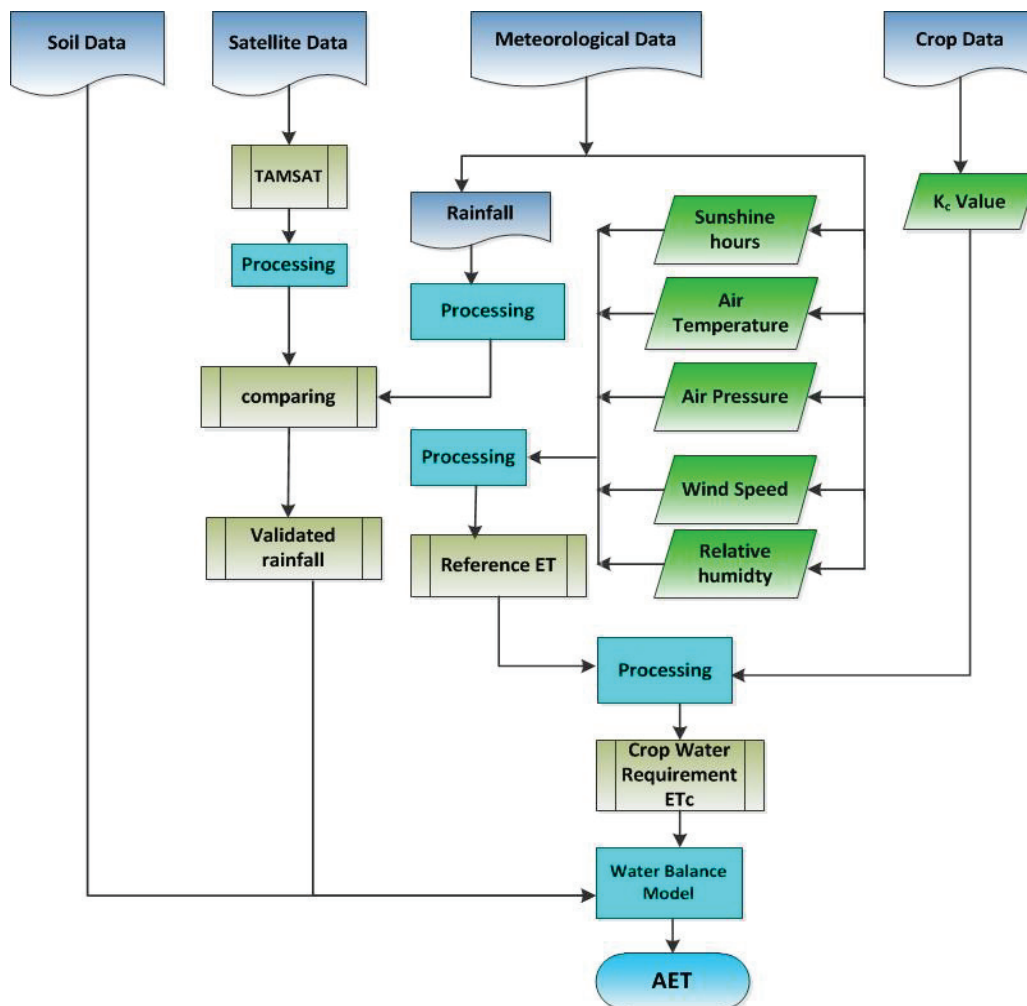


Figure 5-3:-Water Balance Flow Chart

5.4. Estimating AET from SEBS

Models that depend on point measurements give only reliable results at the local scale and are limited in areal extent, due to this estimation of evapotranspiration at a regional scale remain difficult. The surface energy balance (SEBS) model that uses remote sensing data can accurately estimate evapotranspiration from point to continental scale (Su, 2002).

R_n , λE , H , G , H_{wet} and H_{dry} limit, evaporative fraction, AET instantaneous and daily, are the standard outputs of SEBS model. The model estimates those output parameters starting from the general energy balance equation given by

$$R_n = +G_0 + H + \lambda E \quad [\text{W m}^{-2}] \quad 9$$

where R_n -net radiation [W m^{-2}]

G_0 -soil heat flux [W m^{-2}]

H -sensible heat flux, [W m^{-2}]

λE -latent heat flux and [W m^{-2}]

The net radiation the dominant parameter in the energy balance equation was expressed in terms of the balance between incoming and outgoing electromagnetic radiations that is expressed as

$$R_n = (1 - \alpha_0)R_{swd} + \varepsilon R_{lwd} - \varepsilon \sigma T_0^4 \quad [\text{W m}^{-2}] \quad 10$$

where α_0 is surface albedo [-]

R_{swd} is the incoming shortwave radiation [W m^{-2}]

ε is the emissivity of the surface [-]

R_{lwd} Outgoing long wave radiation [W m^{-2}]

T_0 is the land surface temperature [$^{\circ}\text{K}$]

σ is Stefan-Boltzmann constant [$\text{MJ K}^{-4} \text{m}^{-2} \text{day}^{-1}$]

The soil heat flux G_0 was estimated using

$$G_0 = R_n(\Gamma_c + (1 - \text{FVC})(\Gamma_s - \Gamma_c)) \quad [\text{W m}^{-2}] \quad 11$$

where Γ_c and Γ_s are the proportions of soil heat flux and net radiation having value of 0.05 and 0.315 for full vegetation cover and bare soil respectively.

FVC is the fraction of vegetation cover retrieved from LSASAF and this will also be used in the calculation of the roughness length for heat transfer as well as for the calculation of the sensible heat flux.

For the determination of evaporative fraction the energy balance at limiting cases of sensible heat and latent heat fluxes were considered. In this case at the dry limit the latent heat flux approaches to zero and the sensible heat flux is maximum on the other hand at the wet limit is maximum (potential) H is minimum but not zero based on these assumptions the two H limits were estimated

$$H_{dry} = R_n - G_0 \quad [\text{W m}^{-2}] \quad 12$$

$$H_{wet} = R_n - G_0 + \lambda E_{wet} \quad [\text{W m}^{-2}] \quad 13$$

And relative evaporative fraction which is the ratio of actual to potential evapotranspiration was calculated first by

$$\Lambda_r = 1 - \frac{H - H_{\text{wet}}}{H_{\text{wet}} - H_{\text{dry}}} \quad [-] \quad 14$$

From the above the above equation the actual evaporative fraction which is the ratio of latent flux to the available energy (Gibson et al., 2011) was estimated as

$$\Lambda = \frac{\lambda E^* \Lambda_r}{R_n - G_0} \quad [-] \quad 15$$

where Λ is evaporative fraction and Λ_r is the relative evapotranspiration.

The latent heat flux was calculated from the evaporative fraction that was considered as constant for the daily period. The actual sensible heat flux H was computed using meteorological as well as satellite data and is limited with in its dry and wet limits. Wind speed, air temperature and sunshine hours are the required meteorological data, while the surface roughness parameters are the required satellite data.

The sensible heat flux H was computed using Monin-Obukov similarity function starting by estimating the mean wind speed, mean potential temperature and of Obukov length as shown below.

$$u = \frac{u_*}{k} \left(\ln\left(\frac{Z - d_0}{Z_{0m}}\right) - \psi_m\left(\frac{Z - d_0}{L}\right) + \psi_m\left(\frac{Z_{0m}}{L}\right) \right) \quad [\text{m s}^{-1}] \quad 16$$

$$\theta_0 - \theta_a = \frac{H}{k\rho u_* c_p} \left(\ln\left(\frac{Z - d_0}{Z_{0h}}\right) - \psi_h\left(\frac{Z - d_0}{L}\right) + \psi_h\left(\frac{Z_{0h}}{L}\right) \right) \quad [^\circ\text{C}] \quad 17$$

where K is von Karman's constant(0.4) [-]

u is wind speed [m s^{-1}]

θ_0 -potential temperature at the surface [$^\circ\text{C}$]

θ_a -potential temperature at height Z , [$^\circ\text{C}$]

u_* -friction velocity [m s^{-1}]

Z_{0h} -roughness height for heat transfer [m]

Z_{0m} -roughness height for momentum transfer [m]

d_0 -displacement height [m]

L the Obukov length [m]

ψ_m and ψ_h the stability correction function for momentum and heat transfer respectively [-]

In this case Z_{0m} and d_0 were parameterized from canopy height estimated from spot vegetation while the roughness height for heat transfer Z_{0h} was estimated from Z_{0h} and excess resistance to heat transfer $(k_B - 1)$, L the Obukov length in the above equations was estimated

$$L = -\frac{\rho c_p u_*^3 \theta_v}{kgH} \quad [\text{m}] \quad 18$$

Where ρ density of air [kg m^{-3}]

θ_v is the mean virtual temperature [$^\circ\text{C}$]

g is acceleration due to gravity [m s^{-2}]

c_p -specific heat at constant pressure [$\text{MJ kg}^{-1} \text{ }^\circ\text{C}^{-1}$]

Virtual temperature is the temperature that dry air should have in order to have the same density with moist air at given specific humidity (q), temperature (T) and pressure (P) of the air. Based on the equations (16-18) the sensible heat flux H was estimated.

The sensible heat flux at its wet limit was computed from the latent heat flux estimated using a formula similar to Penman Monteith mentioned in equation(4) but with different bulk surface internal resistance r_i which is equal to zero at the wet limit (Su, 2002) and aerodynamic resistance r_e and the above mentioned surface resistances.

Finally having all the above parameters known and considering the evaporative fraction constant throughout the day time the daily actual evapotranspiration of the study area per pixel was easily estimated as follows.

$$E_{daily} = 8.64 * 10^7 \Lambda \frac{R_n^{daily}}{\lambda \rho_w} [\text{mm day}^{-1}] \quad 19$$

In this research before running the SEBS model the study area was divided into 12 ($1^\circ * 1^\circ$) tiles and pre-processing of the input data sets were performed. In this case resampling of the remote sensing and other model output data sets was done to 4 km spatial resolution in order to obtain actual evapotranspiration value having similar spatial resolution with that of the actual evapotranspiration estimated by soil water balance model. Additionally filtering of the LSASAF products was performed in order to have cloud free input parameters and to minimize errors in the output parameters.

5.4.1. Comparing AET from SEBS with Land SAF AET

Prior to the comparison the directly retrieved LSA SAF AET image was resampled to a spatial resolution 4 km and daily temporal resolution in order to have similar resolutions with SEBS output. Additionally the evapotranspiration values from the LSA SAF image at the geo-position that coincides with GPS coordinates collected during field work for the three major crops in the area were extracted using map value operation in ILWIS for the comparison.

The actual evapotranspiration values derived from SEBS and LSA SAF were compared on a pixel basis. However, the agricultural lands on the area are small and it is difficult to find $4*4\text{km}$ agricultural lands covered by identical crop. Accordingly, the comparison was done on relatively homogeneous agricultural areas. Based on this, areas around Adwa, Enderta, and Hintalo districts were selected for Teff, barley and wheat respectively. Finally the comparison was assessed using correlation coefficient R^2 and root mean square errors RMSE (equation 8) to evaluate the performance of the freely available LSA SAF AET for drought monitoring in the study area. The steps followed during the estimation of AET from energy balance are summarized in figure 5-4.

5.5. Comparing WRSI from SEBS with Water Balance

In order to define the variation during the growing season of each crop the model was defined to be estimated every 10 Days. This means that the WRSI value at a particular time during the growing season represents the season-integrated condition from the start of the growing season until the current modeling period. For example, the cumulative values of crop water requirement for two consecutive decades should be 200 mm and only 160 mm was supplied in the form of rainfall, the crop experienced a deficit of 40 mm during the period and thus the WRSI value was calculated as be $(160 / 200) * 100 = 80 \%$.

As mentioned in section 5. WRSI was estimated from AET derived from the LSA SAF and soil water balance as well as crop water requirement estimated from ET_0 and K_c for the three major crops growing

in the study area. The comparison was done after spatially interpolating the WRSI values of each crop from the reliable stations in the area.

Thus, the spatial distribution of WRSI derived from the two methods was compared for the three major crops to evaluate the performance of open source LSA SAF AET from GEONETcast for assessing drought early warning in the area.

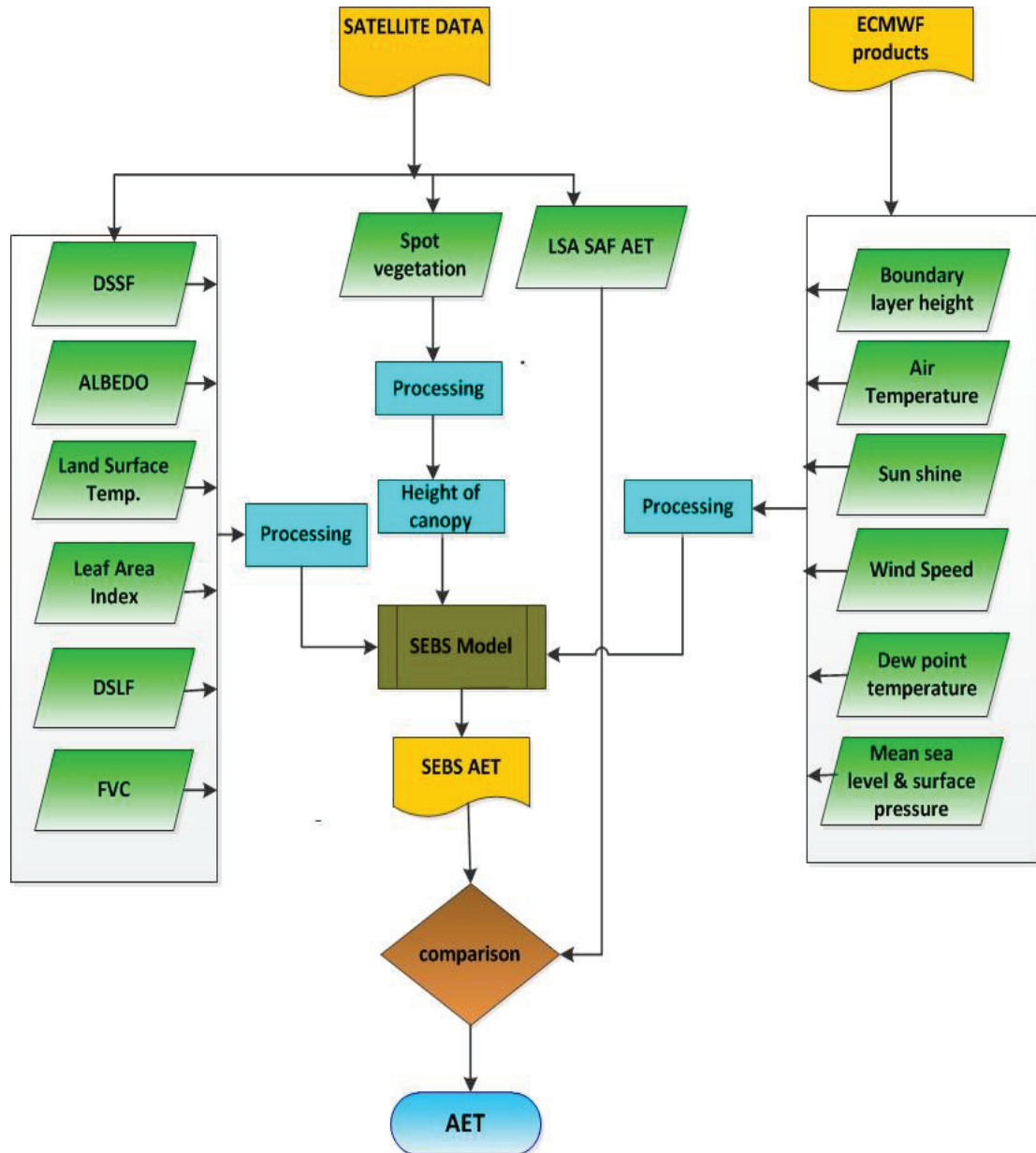


Figure 5-4:-Energy Balance Flow Chart

6. RESULTS AND DISCUSSION

The overall objective of the research was to estimate water requirement satisfaction index for assessment of drought early warning in Tigray region. To achieve this objective rainfall satellite data was validated by in-situ gauge data as mentioned in section 5-3. Consequently actual evapotranspiration was estimated from soil water balance and surface energy balance by integrating real-time satellite data and ground-based ancillary data as summarized in section 5-2 and 5-4. This section presents the results of the analysis performed in the previous sections.

6.1. Rainfall reliability analysis for gauge stations in the study area

A quantitative evaluation of the amount and spatial distribution of precipitation is required for a number of large scale hydrological applications and for mapping rainfall patterns in a specific area. Recently, rainfall measurements from gauge are playing key role in many climatological and hydrological applications. They are still required for operational and calibration rainfall data from satellites and radar. Despite their real time areal representation, rain gauge stations in the study area are too sparse to produce reliable areal estimate. Accordingly, reliability analysis was done to verify the quality of rainfall data collected from the available weather stations. This was conducted on 15 weather stations using double mass curve method. Root mean square error and correlation coefficients were used for this purpose. Out of the 15 weather stations, Shiraro and Maitsebri weather stations show higher RMSE and relatively lower R^2 values, which are resulted from missing data problems. Thus, the two weather stations were omitted for further analysis. The other 13 stations show lower RMSE and higher R^2 values as shown in Table (6.1). These were also used for TAMSAT rainfall data validation. See the correlation graphs on (appendix B).

Table 6-1:-Evaluating the reliability of rainfall stations

Station	R^2	RMSE [mm]
Adigrat	0.98	7.60
Adwa	0.99	2.47
Atsbi	0.98	5.06
Axum	0.98	19.31
Chercher	0.93	10.66
Edaga-Hamus	0.97	2.80
Humera	0.98	3.04
Maichew	0.96	5.69
<i>Maitsebri</i>	<i>0.76</i>	<i>49.76</i>
Mekelle(AP)	0.98	2.21
Mekelle(OB)	0.95	14.15
Rama	0.97	16.83
Senkata	0.98	0.26
<i>Shiraro</i>	<i>0.78</i>	<i>49.73</i>
Shire	0.87	3.07

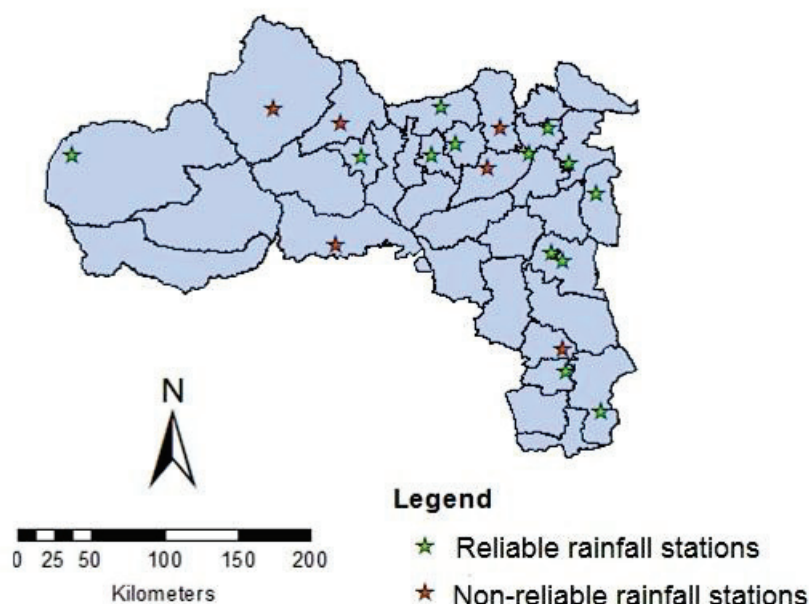


Figure 6-1:-Total rainfall stations of the study area

6.2. Validation of TAMSAT Rainfall Data

Rainfall data collected from weather stations has a limited areal coverage. To alleviate this problem, TAMSAT satellite data was applied due to its higher spatial resolution and its easy access from GEONETcast archive. The TAMSAT rainfall product was validated based on point to pixel as well as pixel by pixel comparison. The correlation Coefficient and root mean square error values for each month within the growing season were mainly used for the comparison.

Table 6-2:-Point to pixel and pixel to pixel comparison results of rainfall data

Month	R ² value	R ² value	RMSE[mm]	RMSE[mm]
	Point-pixel	pixel-pixel	Point-pixel	pixel-pixel
May	0.72	0.58	10.00	32.8
June	0.70	0.71	18.37	18.5
July	0.71	0.68	2.65	28.4
August	0.70	0.82	21.10	15.6
September	0.73	0.84	1.25	5.9

As it is illustrate in Table 6-2 and figure 6-2 the two rainfall data's show comparable results for the whole growing seasons. The RMSE value for the point to pixel comparison varies between 1.25 [mm] and 21.1 [mm] with significant average correlation coefficient value of 0.71. Similarly, RMSE values for pixel to pixel comparison varies from 5.9 to 32.8 [mm] with average correlation coefficient of 0.706. The correlation graph for both comparisons is given in Appendix C&D.

However, the in-situ rainfall data indicate higher values for the entire main growing season (May to September) as compared to that of TAMSAT rainfall products. Underestimated values from the TAMSAT rainfall product is most likely resulted due to the complex topography of the area and the associated orographic rain fall (Beyene & Meissner, 2010). As a result of the complex topography and associated orographic lifting, cloud development can start which in turn leads to start rain while the top cloud temperature is still relatively high. Accordingly, the satellite TAMSAT algorithm only detects after the cloud has released latent heat and develops to a deep convective rainfall.

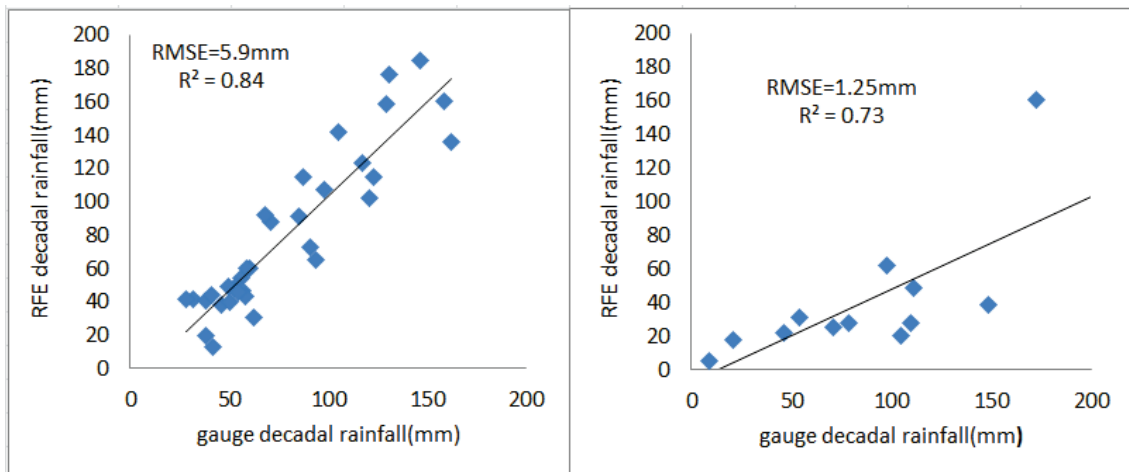


Figure 6-2:-Pixel to pixel (left) and point to pixel (right) Comparison of TAMSAT rainfall with in- situ rainfall for September

6.3. Estimation of Actual Evapotranspiration from Water Balance

Changes in precipitation and temperature patterns result in partitioning of precipitation into actual evapotranspiration (AET), surface runoff, and groundwater recharge. This partitioning of annual precipitation depends on soil water-holding capacity. In this study, the amount of runoff is generally small and was considered as insignificant. In addition, the groundwater table in the study area is deep and hence the capillary rise was not considered.

The actual evapotranspiration trend throughout the growing season was evaluated for three major crops grown in the study area. At the initial growth stage when most part of the soil is not covered by plants, actual evapotranspiration for the three main crops varies between 0 and 20 [mm decade⁻¹] that is much lower than the crop water requirement throughout the study area. During the late developing and mid-season growing stages, AET varies between 20 and 50 [mm decade⁻¹] and approaches the crop water requirement in the western and central part of the study area in particular. However, the actual evapotranspiration value in the southern and eastern part of the study area show frequent fluctuations during the developing and mid stage of growing season and a decreasing trend were observed throughout the mid-season stage. This is mainly due to fluctuations in rainfall distribution that affect the moisture content of the soil.

Though rainfall started late in the western and central part of the study area, it has a good distribution up to the mid-season. While in the eastern and southern parts observed weak rainfall distribution, which strongly affects the soil moisture content and the major food crops grown in the area. Moreover, the soil type of the area has also a great effect to the changes in actual evapotranspiration. The soil type in the western and most of the central parts of the study area is clayey and have higher water holding capacity, which is useful for plants. In contrast, the soil in the other parts of the study has more sandy texture which has lower water holding capacity. The trend for the reference, actual and crop water requirement for the three major crops is illustrated in Figure 6.3.

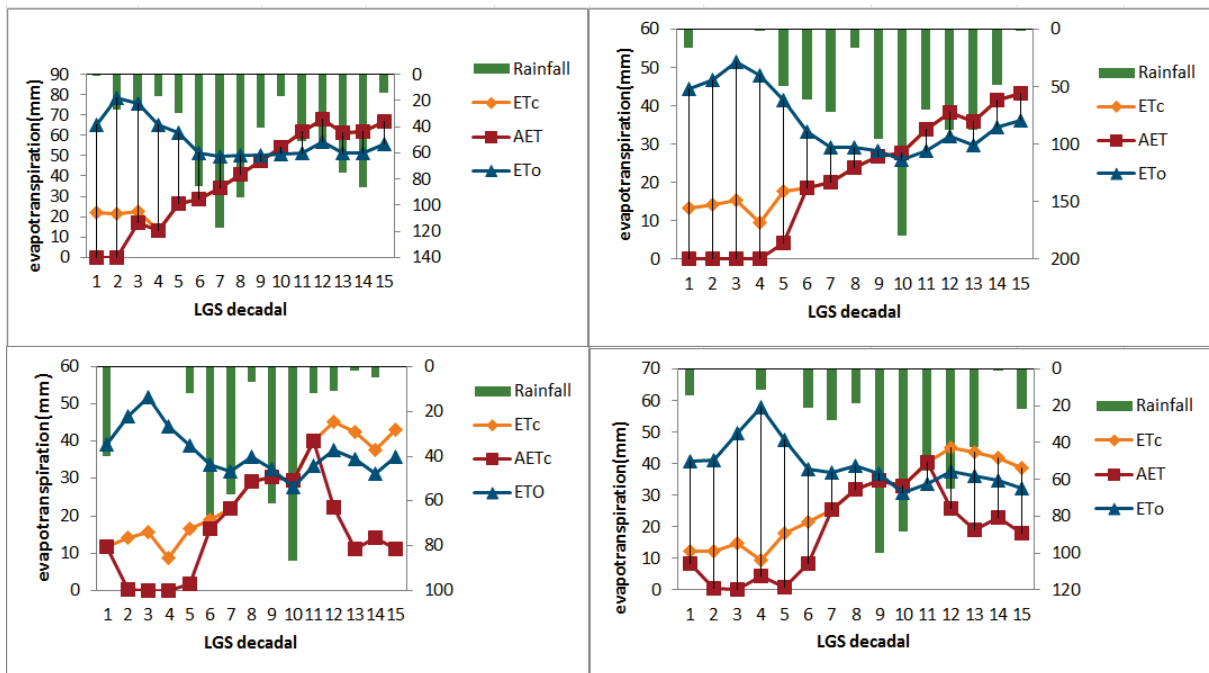


Figure 6-3:- AET trend for Teff in the western (upper left), central (upper right), eastern (lower left) and southern (lower right) parts in relation to ETc and ETo

The reference, actual and crop water requirement trend for the whole growing season of the area for the other crops is given in appendix (D).

Similarly the spatial distribution of actual evapotranspiration estimated from the soil water balance revealed that the three major crops were under water stress especially during the initial and mid-season growing stages in the southern and eastern parts of the area as shown in figure 6-4.

They were also under water stress in the central part during the developing stage. This mainly associates with distribution of rain fall because during the developing stage AET increases and the crop requires sufficient moisture in the soil to compensate the loss of water.

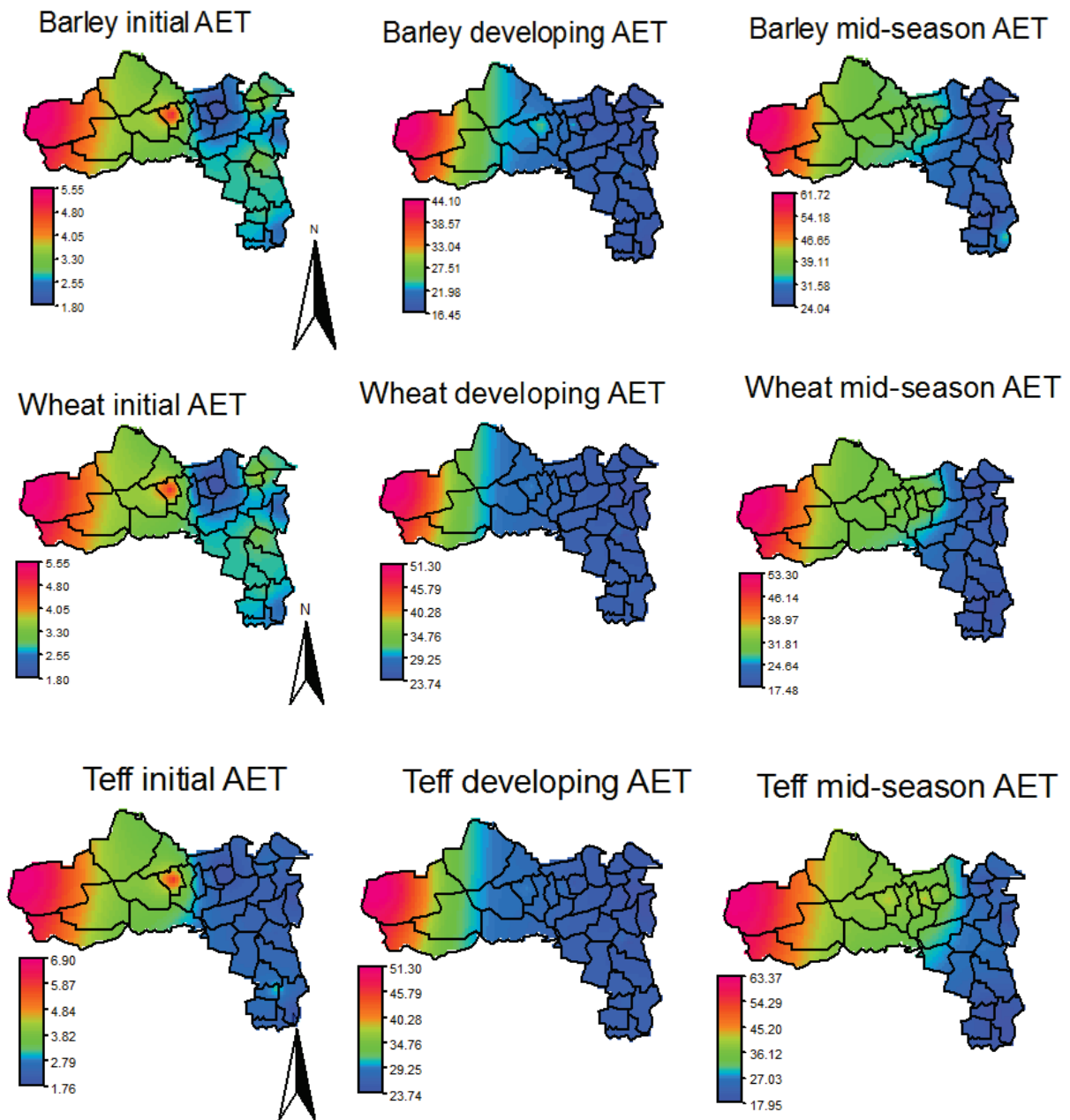


Figure 6-4 :- Spatial distribution of AET for three major crops

6.4. Comparison of AET from SEBS and LSA SAF

Proper estimation of evapotranspiration from root zone is fundamental for crop water deficit and drought mitigation strategies particularly in the arid and semiarid areas where water shortage is a critical problem. Recently, remote sensing based models that rely on land surface energy balance are becoming vital for estimating crop water use both at the field and regional scales. However, the complexities of land surfaces as well as the heterogeneity of the vegetation are making the accuracy of these models difficult. Surface energy balance model which is used to obtain evapotranspiration as a residue from the general energy balance equation, assumes strong dependency actual evapotranspiration value on land surface temperature. This assumption is usually acceptable when evapotranspiration is limited by availability of energy, but this assumption does not hold when evapotranspiration is limited by availability of water in the soil.

Most of the research studies on SEBS model indicated that remote sensing based Surface energy balance overestimate AET particularly on sparsely-vegetated semi-arid regions (Gokmen et al., 2012). This is mainly due to underestimation of sensible heat flux and associate with availability of soil moisture. As discussed in section 5-2 the the study area is characterized by semi-arid climate, shallow rooted rain-fed crops dominated vegetation and relatively deep groundwater. Estimation of AET is therefore strongly associated with availability of water in the soil.

In this study, actual evapotranspiration estimated using SEBS model was compared with Meteosat second generation evapotranspiration product from LSA SAF for the main growing seasons, as shown in figure 6-5 and figure 6-6. Since both methods rely on satellite products which are most likely affected by cloud, the outputs of both products have missing values during the main rainy season. In addition, land surface temperature images had problems during the end of July and mid of August, which resulted a missing output data for SEBS. Notwithstanding the output values of both products have missing values during the main rainy season, actual evapotranspiration values derived from SEBS and LSA SAF were evaluated for the major crops at different areas. However, the comparison was carried out only for the three crops at areas with relatively consistent output.

Accordingly, Adwa, Enderta and Hintalo districts were selected for Teff, barley and wheat respectively for the comparison and this was done by employing correlation coefficient and root mean square errors. The results of the comparison indicated that AET curve illustrate similar trend for the three crops. Moreover, the LSA SAF AET provided relatively higher result during the developing and mid-season growing periods and underestimated values during the initial stage as shown in Figure 6.5. During the developing stage, a small difference between AET values is observed across the three crops. However, a big difference in value was observed during the initial stage for wheat and Teff. Similar difference was also observed during mid-season stage for barley and wheat. As it is illustrated in Figure 6-5, the observed AET values vary between 4.3 and 6.7 [mm day⁻¹] for Teff, and 6.3-9.0 [mm day⁻¹] for wheat at the initial stage. In addition, AET values between 3.8 and 8.8 [mm day⁻¹] and 3.8-7.9 [mm day⁻¹] was observed during the mid-season stage for barley and wheat respectively.

Generally, a relatively higher fluctuation is observed for Teff and this was most likely attributed to topographic effects as the area, Adwa district, is mainly characterized by ragged topography of mountain chains. The findings of the analysis further revealed that the LSA SAF AET provided underestimated result during the start of the season. This is mainly attributed to the algorithms that LSA SAF uses when estimating the actual evapotranspiration. Since the LSA SAF algorithm considers soil moisture at four layers, the soil was dry after prolonged dry periods of about 8 months in the study area due a late start of the rain (Mamo, 2010). It is also observed that LSA SAF AET show an acceptable trend for crop evapotranspiration throughout the growth period. As figure 6-5 (a-c) clearly displays lower AET values was observed during the initial period and then increases during its developing and mid-season stages.

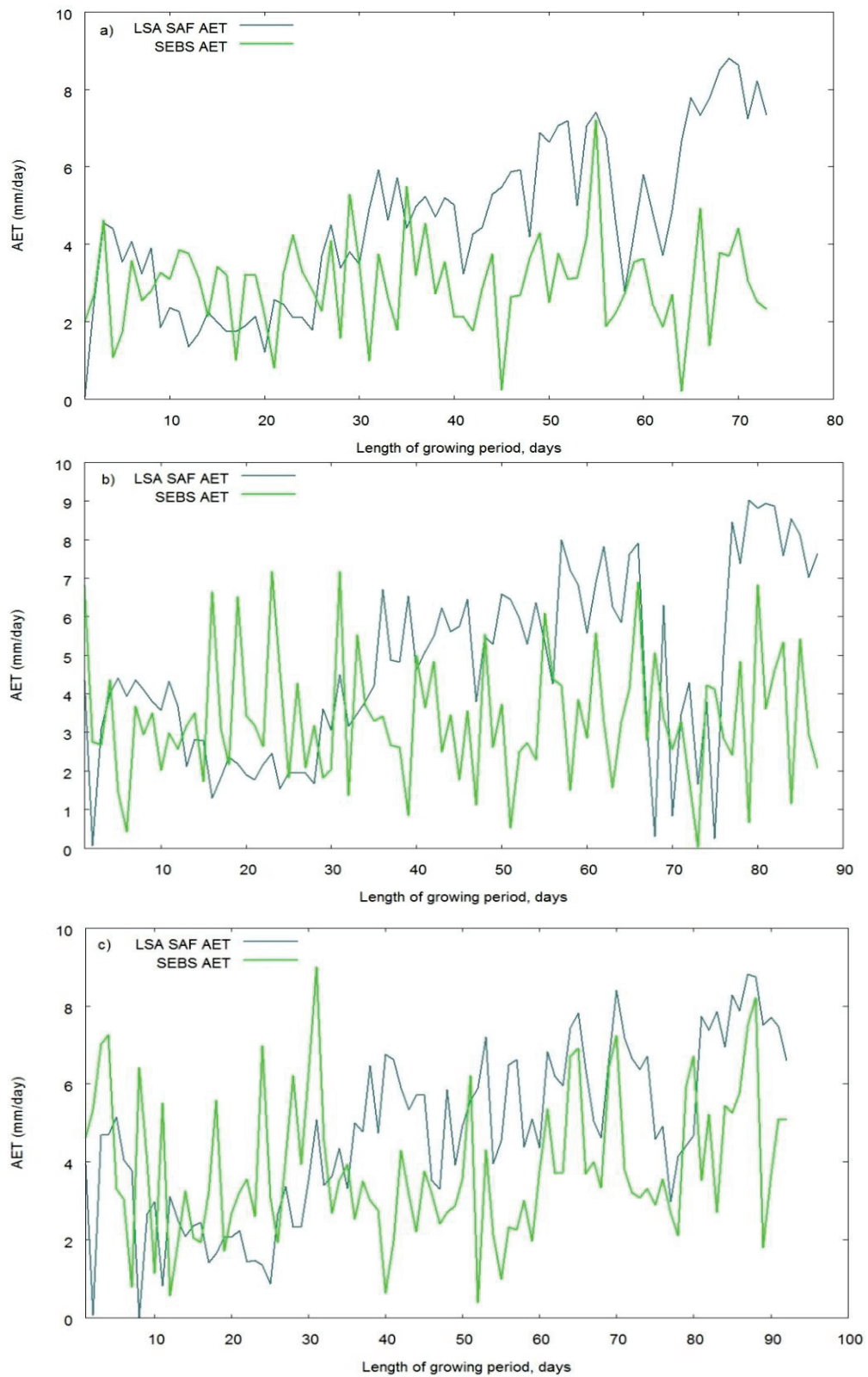


Figure 6-5:-Trend of AET from SEBS and LSA SAF for barley (a), wheat (b) and Teff (c)

Furthermore, R^2 and root mean square error values for the three crops were computed by omitting the anomalies. Accordingly, comparable result was observed for the three stations (Figure 6-6).

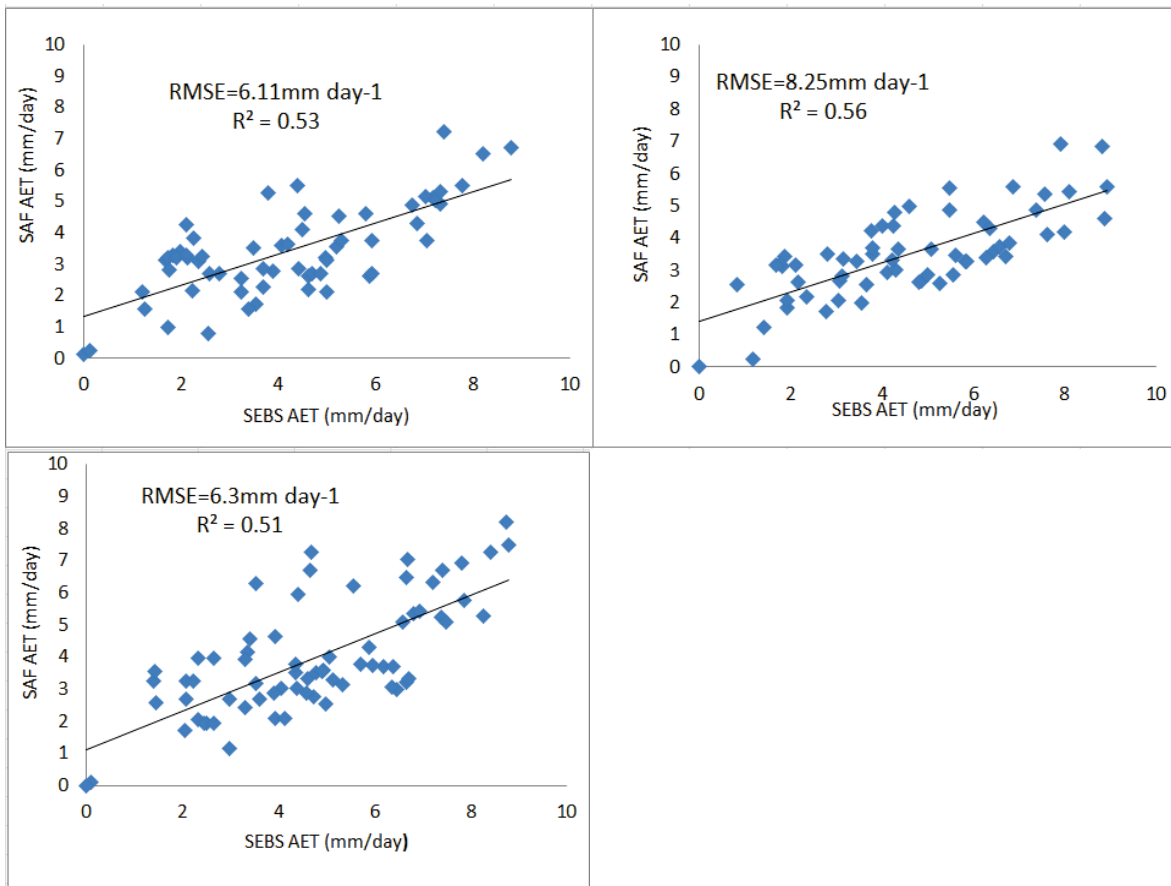


Figure 6-6:-Comparison of SEBS AET with LSA SAF AET for barley (upper left), wheat (upper right) and Teff (lower left) stations

6.5. Comparison of WRSI from Soil water Balance and Energy Balance

The analysis of WRSI for the three major crops growing in the study area was investigated for different planting decades within the growing seasons, i.e. from the first decade of May to the last decade of September using soil water balance and energy balance methods. The performance of the two methods for drought early warning assessment was compared based on the spatial distribution of water requirement satisfaction index.

Based on the water balance method, the spatial distribution of WRSI for barley and wheat show a fluctuation from severe drought to complete crop failure which resulted for the occurrence of drought in the southern and eastern zones of the study area. A WRSI value of less than 60% was obtained in those areas. In contrast, a WRSI value of above 70% was obtained in the central and western zones of the study area indicating a slight to no drought event. Moderate drought trend with a WRSI value of between 60% and 69% was observed in the remaining locations. Similar drought trends were also observed for Teff in the western and central zones of the area. However, a complete crop failure was observed in some pocket areas of the southern and eastern zones.

Similar trends of WRSI distribution was observed for the three crops by employing the energy balance method. Based on this method, a WRSI value of less than 60% for Teff was only observed in few areas of

the southern and eastern zones, indicating a severe drought to complete crop failure. Similar result was observed for barley and wheat in small areas of the central part of the study area. Moderate drought trend with a WRSI value of 60-69% was dominantly observed for barley and wheat in the central and some south eastern zones of the study area. The same result was also dominantly observed in the central, eastern and southern zones for Teff.

Slight drought trend with a WRSI value of 70-79% was observed in western and some areas in the central and south eastern part for the three crops. Moreover, a WRSI value between 80% and 100% was obtained from the water balance in the western part of the study area, which indicates a no drought trend. This result was not observed with the energy balance model as illustrated in figure 6-7. The reason is most likely due the problems of cloud cover. Examining the rainfall trend in the western part of study area indicates a high rainfall distribution and this in turn strongly affects the satellite that resulted to underestimate LSA SAF AET.

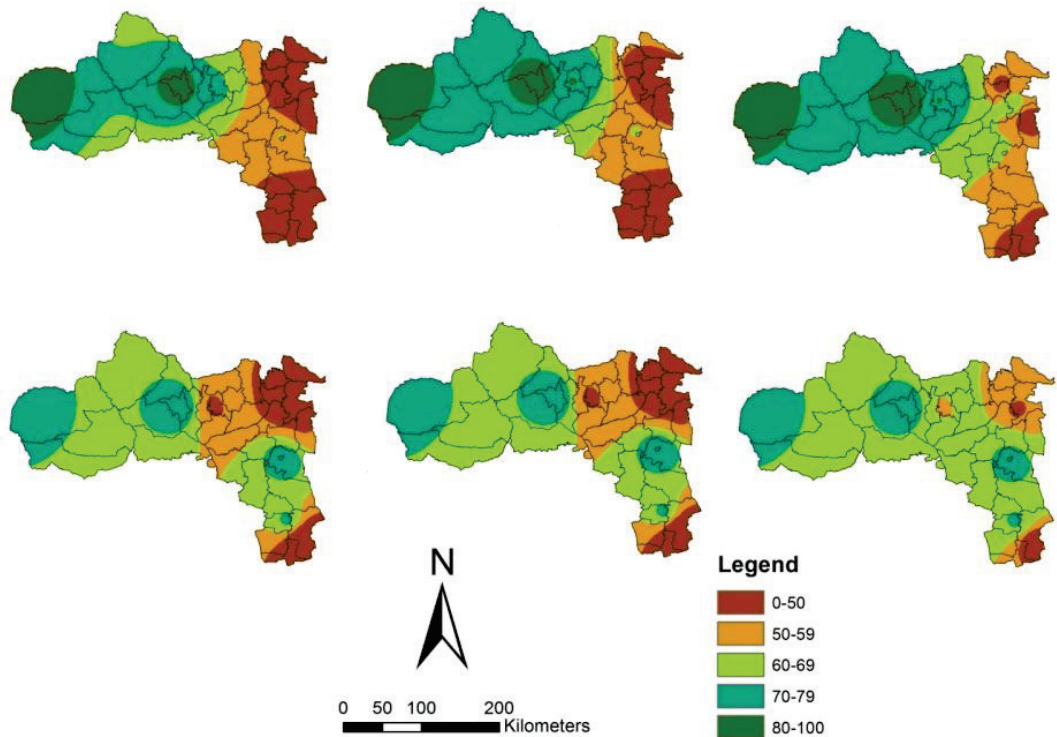


Figure 6-7:-Spatial distribution of WRSI for barley, wheat and Teff (left to right) derived from soil water balance (upper) and energy balance (lower)

7. CONCLUSIONS AND RECOMMENDATION

7.1. Conclusion

The aim of this research was to compare WRSI derived from soil water balance and energy balance, which aids to improve assessment of localized drought in Tigray region, northern Ethiopia. To meet this objective, satellite rainfall data was validated with in-situ gauge data. Accordingly, actual evapotranspiration was estimated using soil water balance and energy balance methods by employing meteorological and satellite data from GEONETcast. Based on the two methods, the spatial distribution of WRSI in the study area was examined. This section presents the conclusions and discussion of the main findings of this study.

In this work geostationary satellite products and ground based meteorological data were employed to estimate WRSI from soil water balance and energy balance for three major rain-fed crops in the study area. The advantages of relatively higher spatial resolution rainfall, surface parameters and other radiation products from EUMETSAT geostationary satellite were fully utilized. The combined use of those products enabled to get all model input parameters with the required temporal and spatial resolution, which was used to estimate AET using the two models.

Reliability analysis based on double mass curve techniques was conducted at a station level using in-situ rainfall gauge daily basis data acquired from NMA from 15 weather stations during the rainy season, May-Sep 2012. The double mass curve analysis revealed that majority of the rainfall stations provides a consistent data. However, some stations located in the North West and south west parts of the study area were dropped from the analysis due to inconsistency of data recording. Therefore, the in-situ rainfall gauge data from the reliable stations can be used for operational and calibration of rainfall data from satellites.

Based on the above point, the in-situ rainfall gauge data from the reliable weather stations were selected for the validation of satellite rainfall estimates. Consequently, a station point rainfall to satellite pixel rainfall as well as in-situ pixel to satellite pixel rainfall comparison was performed. The results showed that the two comparison methods (point to pixel, pixel to pixel) at the 13 reliable weather stations gave comparable results. This indicates the TAMSAT rainfall estimates can provide appropriate near real time information results for the estimation of AET using a soil water balance and to analyze the state of crops from the status of the actual soil moisture content. Similar results were reported by Beyene & Meissner (2010).

Actual evapotranspiration estimated using water balance approach show an increasing trend with increasing of precipitation indicating the increase in precipitation intensifies the water cycle and suppress drought in the area. For this reason the estimated AET was varying more with rainfall distribution and deviated more from the crop water requirement in the eastern and southern zones of the study area particularly during the developing and mid stages of the crop. This indicates a deficiency of moisture in the soil and the crops were under water stress. In contrast, AET was smoothly increasing and approached to the crop water requirement in the central and western zones of the study area implying existence of enough moisture in the soil to hold crops during the developing and mid-season stages. Therefore, water balance method can provide reasonable estimates of AET distribution for rain-fed crops which in turn aids accurate assessment of drought.

The findings of the comparison between SEBS AET and LSA SAF AET showed similar spatial and temporal distribution with a good correlation for the three major crops in the area. Moreover, the LSA SAF AET showed similar trend with the water balance estimate of AET. Therefore, it can provide reliable estimate AET for proper assessment of drought in near real time (Ghilain et al.).

Finally, Water Requirement Satisfaction Index was calculated using GEONETcast and in-situ data at station level. Accordingly, the spatial and temporal characteristics of drought were analyzed for wheat, barley and Teff by comparing the performance of energy balance and soil water balance model outputs. The finding clearly indicated that water balance model is strongly dependent on rainfall and higher WRSI values were observed in areas with high rainfall distribution. In contrast, the energy balance model showed underestimated WRSI value in the areas of higher rainfall distribution mainly due to problems cloud cover effects. The findings further revealed that WRSI estimates based on the water balance method lacks spatial extent that resulted irregular values with in a similar agro-ecologic areas. While the energy balance method result showed a smoothly distributed WRSI values with relatively less anomalies. This indicates the energy balance can provide appropriate estimates of WRSI for proper monitoring of drought early warning during cloud free days. However, during existence of cloud cover, water balance method is an appropriate alternative for drought monitoring.

7.2. Recommendation

Based on the findings of this research the following points are recommended

- ✓ Despite their spatial coverage limitation, the availability of consistent ground truth data is important for the validation of remote sensing derived satellite data. Thus extensive field observation with comprehensive survey of hydrological and surface parameters is recommended to improve the accuracy of drought assessment.
- ✓ The meteorological weather stations in the area are too sparse for representation of the whole region and to validate the satellite data. Therefore assessing drought at lower administrative districts can provide better accuracy.
- ✓ The FAO digital soil classification used for this study has coarser spatial resolution and this can combine soils of different texture in to a single soil type. This affected the estimation of the water holding capacity of the soil and accordingly the estimation of AET from water balance. Therefore, soil moisture classification with higher spatial resolution can provide better estimates of WRSI for accurate monitoring of drought.
- ✓ In this study the analysis was limited for the rainy months only and during those months the cloud cover had a great effect on satellite estimates of AET, so extending the time of analysis can provide better estimates of AET from cloud free pixels ,this will increase the accuracy of drought assessment in the area.
- ✓ Direct methods of ET measurements such as pan-measurement, Bowen ratio, eddy correlation system, and weighing lysimeter at a station level are required for the validation of satellite based AET estimate.
- ✓ The satellite data used in this research had spatial resolution of 4 km, however the agricultural land cultivated with rain-fed crops in the study area have smaller size. Integrating satellite data with the exact location of the plot of land where the rain-fed crops are growing can provide better understanding on the occurrence of drought. Therefore detailed land use classification is recommended for accurate drought assessment at a single crop level.

LIST OF REFERENCES

- Allen, R. G., Pereira, L. S., Raes, D., & Smith, S. (1998). *Crop Evapotranspiration - Guidelines for computing crop water requirements - FAO Irrigation and Drainage paper NO. 56*. Rome, Italy: Food and Agriculture Organization of the United Nations (FAO).
- Allen, R. G., Pereira, L. S., Smith, M., Raes, D., & Wright, J. L. (2005a). FAO-56 dual crop coefficient method for estimating evaporation from soil and application extensions. *Journal of Irrigation and Drainage Engineering-Asce*, 131(1), 2-13.
- Allen, R. G., Pruitt, W. O., Raes, D., Smith, M., & Pereira, L. S. (2005b). Estimating evaporation from bare soil and the crop coefficient for the initial period using common soils information. *Journal of Irrigation and Drainage Engineering-Asce*, 131(1), 14-23.
- Araya, A., & Stroosnijder, L. (2011). Assessing drought risk and irrigation need in northern Ethiopia. *Agricultural and Forest Meteorology*, 151(4), 425-436.
- Araya, A., Stroosnijder, L., Girmay, G., & Keesstra, S. D. (2011). Crop coefficient, yield response to water stress and water productivity of teff (*Eragrostis tef* (ZUCC.)). *Agricultural Water Management*, 98(5), 775-783.
- Ataklti, T. Y. (2012). *Assessing the potential of Geonetcast earth observation and in-situ data for drought early warning and monitoring in Tigray, Ethiopia*. University of Twente Faculty of Geo-Information and Earth Observation (ITC), Enschede.
- Ayse, I. (2008). Estimation of Land Surface Energy Fluxes: An Application of Satellite Remote Sensing Procedure *World Environmental and Water Resources Congress 2008* (pp. 1-10): American Society of Civil Engineers.
- Behera, S. K., Luo, J.-J., Masson, S., Delecluse, P., Gualdi, S., Navarra, A., & Yamagata, T. (2005). Paramount Impact of the Indian Ocean Dipole on the East African Short Rains: A CGCM Study. *Journal of Climate*, 18(21), 4514-4530.
- Beyene, E. G., & Meissner, B. (2010). Spatio-temporal analyses of correlation between NOAA satellite RFE and weather stations' rainfall record in Ethiopia. *International Journal of Applied Earth Observation and Geoinformation*, 12, Supplement 1(0), S69-S75.
- Biggs, T. W., Mishra, P. K., & Turrall, H. (2008). Evapotranspiration and regional probabilities of soil moisture stress in rainfed crops, southern India. *Agricultural and Forest Meteorology*, 148(10), 1585-1597.
- BOFED. (2004). *National Regional State of Tigray Strategic Plan for the years 2004-2006*.
- Boken, V. K. (2009). Improving a drought early warning model for an arid region using a soil-moisture index. *Applied Geography*, 29(3), 402-408.
- Brown, M. E. (2008). FEWS NET's Structure and Remote Sensing Famine Early Warning Systems and Remote Sensing Data (pp. 41-61): Springer Berlin Heidelberg.
- CSA. (2008). Summary and Statistical Report of the 2007 Population and Housing Census, Federal Democratic Republic of Ethiopia Population Census Commission.
- Diao, X. (2010). Economic Importance of Agriculture for Sustainable Development and Poverty Reduction: The Case Study of Ethiopia. Global Forum on Agriculture 29-30 November 2010, Policies for Agricultural Development, Poverty Reduction and Food Security OECD Headquarters, Paris.
- Edossa, D., Babel, M., & Das Gupta, A. (2010). Drought Analysis in the Awash River Basin, Ethiopia. *Water Resources Management*, 24(7), 1441-1460.

- Elhag, M., Psilovikos, A., Manakos, I., & Perakis, K. (2011). Application of the Sebs Water Balance Model in Estimating Daily Evapotranspiration and Evaporative Fraction from Remote Sensing Data Over the Nile Delta. *Water Resources Management*, 25(11), 2731-2742.
- FAO. (2007). FAO Irrigation and Drainage Paper No. 56 Crop Evapotranspiration: Guidelines for computing crop water requirements. Accessed December 16, 2012 from <http://www.kimberly.uidaho.edu/ref-et/fao56.pdf>.
- Gebrehiwot, T., van der Veen, A., & Maathuis, B. (2011). Spatial and temporal assessment of drought in the Northern highlands of Ethiopia. *International Journal of Applied Earth Observation and Geoinformation*, 13(3), 309-321.
- Gelassie, T. Y. (2012). *Remote sensing evapotranspiration using geonetcast and in situ data streams for drought monitoring and early warning : case study for the Amhara region in Ethiopia*. University of Twente Faculty of Geo-Information and Earth Observation (ITC), Enschede.
- Ghilain, N., Arboleda, A., & Gellens-Meulenberghs, F. Monitoring evapotranspiration at sub-kilometer scale: Downscaling MSG/SEVIRI images using moderate resolution remote sensing derived data.
- Gibson, L., Münch, Z., & Engelbrecht, J. (2011). Particular uncertainties encountered in using a pre-packaged SEBS model to derive evapotranspiration in a heterogeneous study area in South Africa. *Hydrology and Earth System Sciences*, 15(1), 295-310.
- Glantz, M. H. (2001). *Currents of change: EL NIÑO'S impact on climate and society*. (Second Edition ed. Vol.). Cambridge, United Kingdom: Cambridge University Press
- Gokmen, M., Vekerdy, Z., Verhoef, A., Verhoef, W., Batelaan, O., & van der Tol, C. (2012). Integration of soil moisture in SEBS for improving evapotranspiration estimation under water stress conditions. *Remote Sensing of Environment*, 121(0), 261-274.
- Hagos, F., Pender, J., & Gebresselassie, N. (1999). Land degradation in the highlands of Tigray and strategies for sustainable land management. Socioeconomic and Policy Research Working Paper No. 25: International Livestock Research Institute.
- Haile, T. (1988). Causes and Characters of Drought in Ethiopia. *Ethiopian Journal of Agricultural Sciences*.
- Heim, R. R. (2002). A Review of Twentieth-Century Drought Indices Used in the United States. *Bulletin of the American Meteorological Society*, 83(8), 1149-1165.
- Li, Z.-L., Tang, R., Wan, Z., Bi, Y., Zhou, C., Tang, B., . . . Zhang, X. (2009). A Review of Current Methodologies for Regional Evapotranspiration Estimation from Remotely Sensed Data. *Sensors*, 9(5), 3801-3853.
- Liu, M., Bardossy, A., Li, J., & Jiang, Y. (2012). Physically-based modeling of topographic effects on spatial evapotranspiration and soil moisture patterns through radiation and wind. [JOURNAL]. *Hydrological Earth System Science*, 16(2).
- Maathuis, B., Mannaerts, C., & Retsios, B. (2008). The ITC GEONETCast-toolbox approach for less developed countries. *Proceedings of Commission VII*, 37, 1301-1306.
- Maathuis, B. H. P., Mannaerts, C., Schouwenburg, M., Retsios, B., & Lemmens, R. (2010). Instalation, Configuration and user guide of the GEONETcast toolbox plug-in for ilwis 3.7. Available at <http://52north.org/files/earth-observation/userguides/gnc/gnc> Last retrieved on 28 July 2012.
- Mamo, T. A. (2010). Estimation of Actual Evapotranspiration and Water Balance Using Combined Geostationary and Polar Orbiting Satellite Products: A Case Study in Spain.
- Mannaerts, C. M., Maathuis, B. H. P., Molenaar, M., & Lemmens, R. L. G. (2009). ITC GEONETCast toolbox : a geo capacity building component for education and training in global earth observation and geo information provision to society. In: *IGARSS 2009 : Proceedings of the 2009 IEEE international geoscience and remote sensing symposium : Earth observation, origins and applications, July 12-17, 2009, Cape Town, South Africa*, ISBN 978-1-4244-3395-7 pp. V 385 - V 388.

- Mishra, A. K., & Singh, V. P. (2010). A review of drought concepts. *Journal of Hydrology*, 391(1–2), 202-216.
- Nyssen, J., J. Poesen, J. Moeyersons, J. Deckers, M.H., & Lang, A. (2004). Human impact on the environment in the Ethiopian and Eritrean highlands- state of the art. *Earth-Science Review*, 64, 273-320.
- Nyssen, J., Poesen, J., Haile, M., Moeyersons, J., Deckers, J., & Hurni, H. (2009). Effects of land use and land cover on sheet and rill erosion rates in the Tigray highlands, Ethiopia. *Zeitschrift für Geomorphologie*, 53(2), 171-197.
- Pender, J., Ssewanyana, S., Kato, E., & Nkonya, E. (2004). Linkages between poverty and land management in rural Uganda: Evidence from Uganda National Household Survey, 1999/00. EPTD Discussion Paper No. 122. Environment and Production Technology Division, International Food Policy Research Institute (IFPRI), Washington, DC.
- Reynolds, C. A., Yitayew, M., Slack, D. C., Hutchinson, C. F., Huete, A., & Petersen, M. S. (2000). Estimating crop yields and production by integrating the FAO Crop Specific Water Balance model with real-time satellite data and ground-based ancillary data. *International Journal of Remote Sensing*, 21(18), 3487-3508.
- Senay, G. B. (2008a). Landscape evapotranspiration estimation using remotely sensed data for operational applications in agriculture and hydrology. *Contributions of satellite remote sensing to drought monitoring, National Integrated Drought Information System Knowledge Assessment Workshop*.
- Senay, G. B. (2008b). Modeling Landscape Evapotranspiration by Integrating Land Surface Phenology and a Water Balance Algorithm. *Algorithms* 1(2), 52-68.
- Senay, G. B., Leake, S., Nagler, P. L., Artan, G., Dickinson, J., Cordova, J. T., & Glenn, E. P. (2011). Estimating basin scale evapotranspiration (ET) by water balance and remote sensing methods. *Hydrological Processes*, 25(26), 4037-4049.
- Simmons, A., Uppala, S., Dee, D., & Kobayashi, S. (2007). ERA-Interim: New ECMWF reanalysis products from 1989 onwards. *ECMWF newsletter*, 110, 25-35.
- Su, Z. (1999). The Surface Energy Balance System (SEBS) for estimation of turbulent heat fluxes. *Hydrology and Earth System Sciences*, 6(1), 85-100.
- Su, Z. (2002). The Surface Energy Balance System (SEBS) for estimation of turbulent heat fluxes. *Hydrology and Earth System Sciences*, 6(1), 85-99.
- Tesfay, G. (2006). *Agriculture, Resource Management and Institutions A socioeconomic analysis of households in Tigray, Ethiopia. PhD Thesis, Wageningen University*.
- Thorne, V., Coakley, P., Grimes, D., & Dugdale, G. (2001). Comparison of TAMSAT and CPC rainfall estimates with raingauges, for southern Africa. *International Journal of Remote Sensing*, 22(10), 1951-1974.
- Trigo, I. F., Dacamara, C. C., Viterbo, P., Roujean, J.-L., Olesen, F., Barroso, C., . . . Arboleda, A. (2011). The Satellite Application Facility for Land Surface Analysis. *International Journal of Remote Sensing*, 32(10), 2725-2744.
- Wilhite, D. A., & Glantz, M. H. (1985). Understanding: the Drought Phenomenon: The Role of Definitions. *Water International*, 10(3), 111-120.

LIST OF APPENDICES

Appendix-A: -Pre-processing steps of Penman-Monteith equation for the calculation of Reference evapotranspiration

Vapour pressure:- is the amount of water vapour in the air that contributes its pressure to the total pressure of the atmosphere and was parameterized as saturated and actual.

Saturated vapour pressure (e_s) (kpa):- the pressure at which the water molecules escaping from returning to the evaporating surface from the atmosphere reached equilibrium and was estimated by

$$e_s = \frac{e^0(T_{\max}) + e^0(T_{\min})}{2} \quad 1$$

where $e^0(T)$ is saturation vapour pressure at the air temperature T (kPa) this was given by

$$e^0(T) = 0.611e^{\left(\frac{17.27T}{T+237.3}\right)} \quad 2$$

T is air temperature ($^{\circ}\text{C}$)

Actual vapour pressure (e_a) (kPa):- is the vapour pressure exerted by the water vapour in the air. It can be calculated by different formulas, but for this case it was calculated using mean relative humidity of the area which is given by

$$e_a = \frac{RH_{\text{mean}}}{100} \left[e_s \frac{e^0(T_{\max}) + e^0(T_{\min})}{2} \right] \quad 3$$

where RH is the mean relative humidity (%)

The vapour pressure deficit an indicative of the actual evaporative capacity of the air was determined from difference between the saturation and actual vapour pressure.

$$e_s - e_a \quad 4$$

Net Radiation (Rn) (MJ/ m²day):- is the difference between the incoming net shortwave (Rns) wave radiation and the Outgoing net long wave radiation (Rnl). For the parameterization of this net radiation from the collected meteorological data different steps were undertaken

Extraterrestrial radiation Ra (MJ/ m²day):- the radiation received at the top of the earth's atmosphere on a horizontal surface is defined as a function of each day of the year as well as different latitudes (Allen et al., 2005a). This was estimated from solar constant, declination angle of the sun and time of the year.

$$R_a = \frac{24(60)}{\pi} G_{sc} d_r (\omega_s \sin(\varphi) \sin(\delta) + \cos(\varphi) \cos(\delta) \sin(\omega)) \quad 5$$

where Ra extraterrestrial radiation

G_{sc} -solar constant is the radiation striking the surface perpendicular to the sun's ray which is equal to 0.0820 MJ /m² min

d_r inverse relative distance Earth-Sun which was estimated by the formula

$$d_r = 1 + 0.033 \cos\left(\frac{\pi}{365} * J\right) \text{ J is the Julian date which starts 1 from January.}$$

ω - Sunset hour angle (rad) calculated by

$$\omega_s = \arccos(-\tan(\varphi)\tan(\delta)) \quad 6$$

φ latitude (rad)

δ solar declination angle (rad), which is calculated by

$$\delta = 0.409 \sin\left(\frac{2\pi}{365} J - 1.39\right) \quad 7$$

Solar or shortwave radiation (Rs) The amount of radiation reaching the Earth after being reflected absorbed and scattered by atmospheric gases. This was parameterized using Angstrom formula given as

$$R_s = \left(a_s + b_s \frac{n}{N}\right) R_a \quad 8$$

where R_s - solar radiation MJ /m² day)

n -actual sunshine duration (hour)

N - Daylight hours (hour)

$\frac{n}{N}$ -relative sunshine duration

$a_s + b_s$ -fraction of extraterrestrial radiation reaching the earth during cloudless days and are represented by constant numbers of 0.25 and 0.5 respectively

After the estimation of solar or short wave radiation from the above formula the calculation for the net short wave radiation which is the fraction of radiation not reflected from the surface was estimated from the constant albedo of the reference surface and solar radiation using

$$(1 - \alpha)R_s \quad 9$$

where α is the surface albedo.

Furthermore the net long wave radiation which is the difference between the outgoing and incoming long wave radiations was also estimated using the Stefan-Boltzmann law

$$R_{nl} = \sigma \left(\frac{T_{\max}^4 - T_{\min}^4}{2} \right) (0.34 - 0.14\sqrt{e_a}) \left(1.35 \frac{R_s}{R_{so}} - 0.35 \right) \quad 10$$

where, R_{nl} net outgoing long wave radiation (MJ /m² day)

σ -Stefan-Boltzmann constant (4.903 10⁻⁹ MJ /K⁴ m² day¹)

T_{\max} - maximum temperature (K)

T_{\min} -minimum temperature (K)

E_a - actual vapour pressure (kPa)

R_s/R_{so} relative shortwave radiation

R_s -solar radiation (MJ /m² day¹)

R_{so} -clear-sky radiation (MJ m² day¹) estimated by

$$R_{so} = (a_s + b_s) R_a \quad 11$$

Finally the net radiation of the reference surfaces in each station in the study area was calculated as the difference between the net incoming short wave radiation and outgoing long wave radiation. According to the (Allen et al., 2005a) the soil heat flux for daily and decadal is very small and the reference evapotranspiration was calculated for daily time scale. Based on this assumption the daily soil heat flux (G) was considered zero.

Other parameters used for the calculation of ET₀ includes the Psychrometric constant (γ), Slope of saturation vapour pressure curve (Δ) and Latent heat of vaporization (λ)

The Psychrometric constant (γ) is characterized as a function of air pressure and was estimated simply using

$\gamma = 0.665 * 10^{-3} P$ (Kpa/0c) where p is the air pressure which varies according to the elevation of the stations and was calculated by the following formula

$$P = 101.3 \left(\frac{293 - 0.0065Z}{293} \right)^{5.26} \quad 12$$

The slope of saturated vapour pressure (Δ) (Kpa) for each station in the study area was calculated as a function of mean air temperature as follows

$$\Delta = 4098 \frac{0.6108 \left(\frac{17.27T}{T+237.3} \right)}{(T+237.3)^2} \quad 13$$

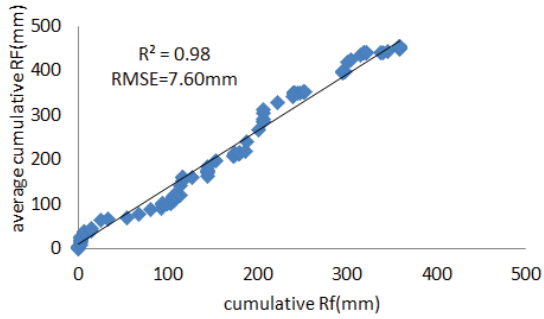
In the study area out of the 15 weather stations there were 2 weather stations having missed data of some parameters such as relative humidity and sunshine hours, for those stations the reference evapotranspiration was calculated using different procedure. In this case the ET₀ was calculated using the formula used by FAO Hargreaves ET₀ equation for missing weather data and this was used the estimation of ET₀ in the two weather stations.

This requires only the maximum and minimum temperature and is given by

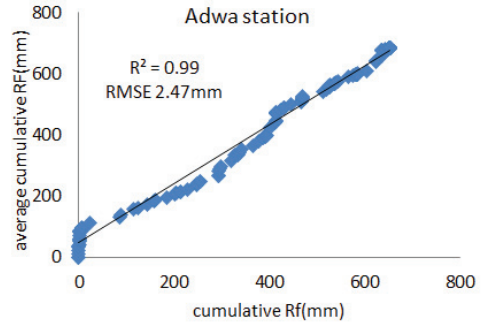
$$ET_0 = 0.0023(T_{\text{mean}} + 17.8)(T_{\text{max}} - T_{\text{min}})^2 R_a \quad [\text{MJ} / \text{m}^2 \text{ day}] \quad 14$$

Appendix-B: - Scatter plot showing Reliability evaluation of rainfall stations using double mass curve method.

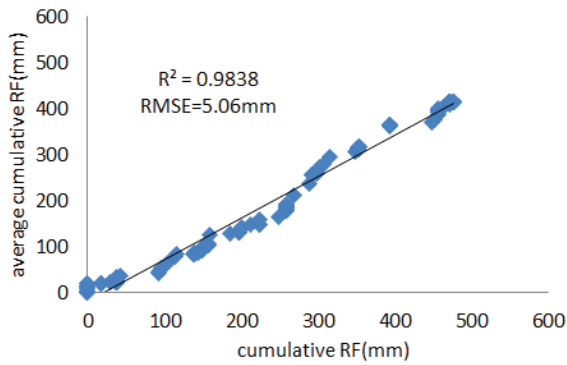
Adigrat station



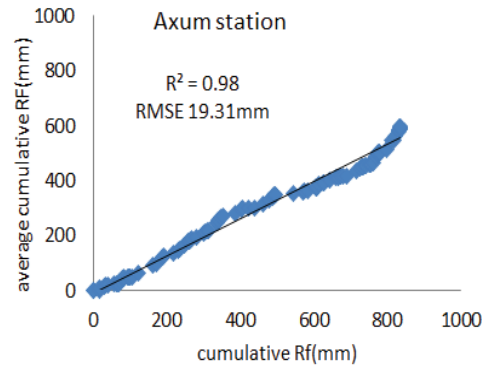
Adwa station



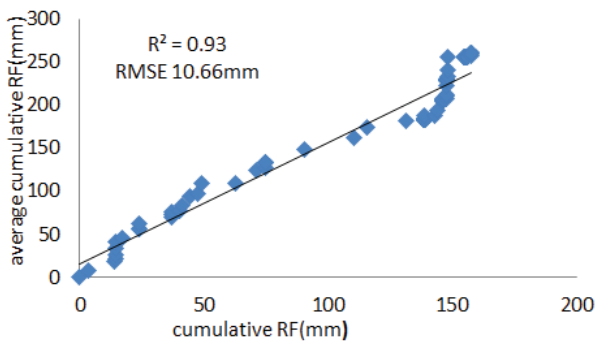
Atsbi station



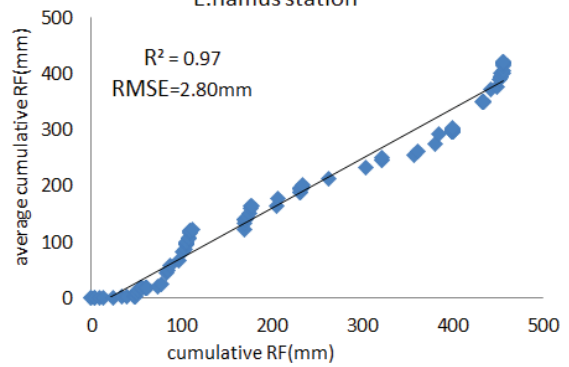
Axum station

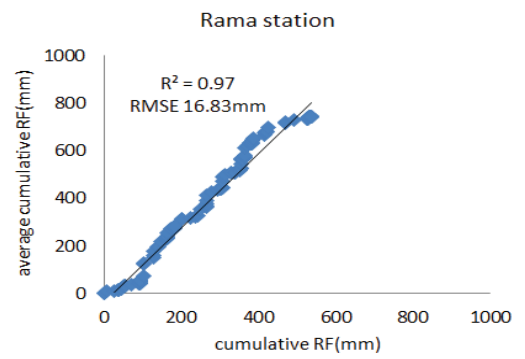
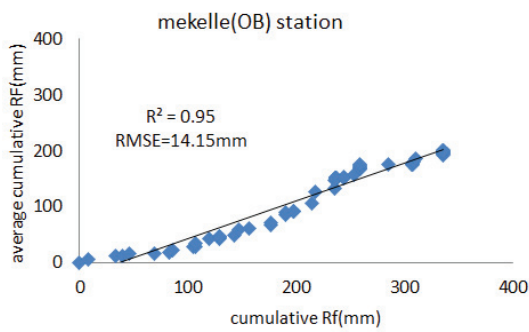
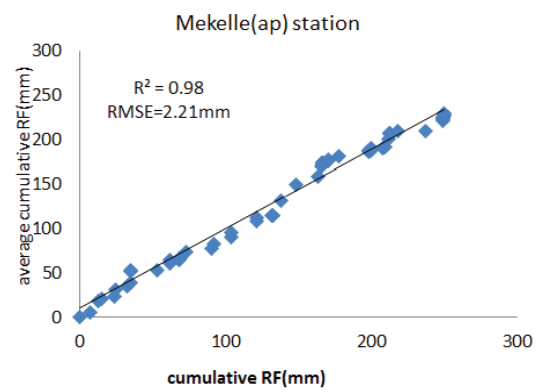
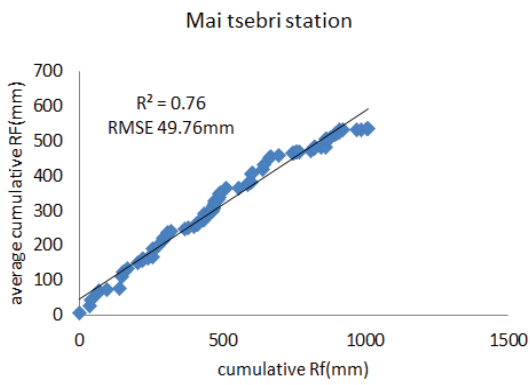
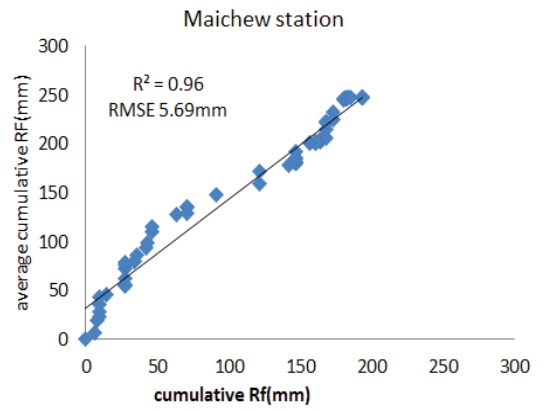
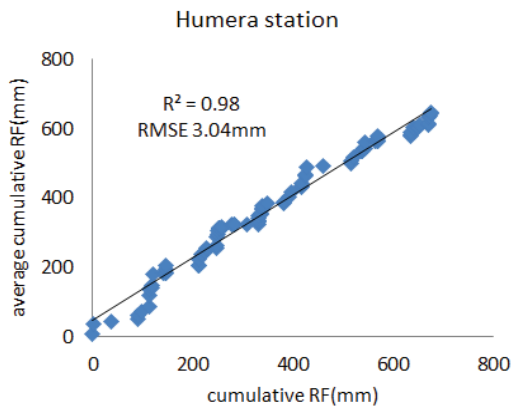


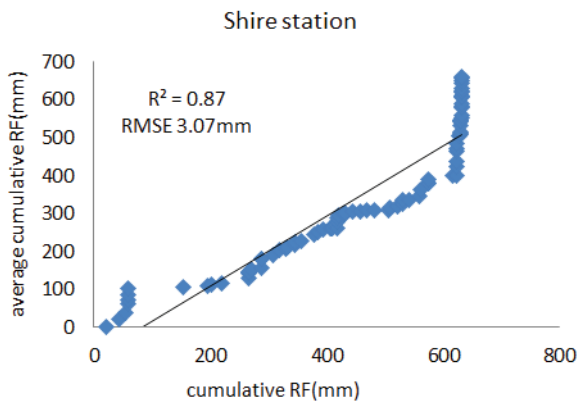
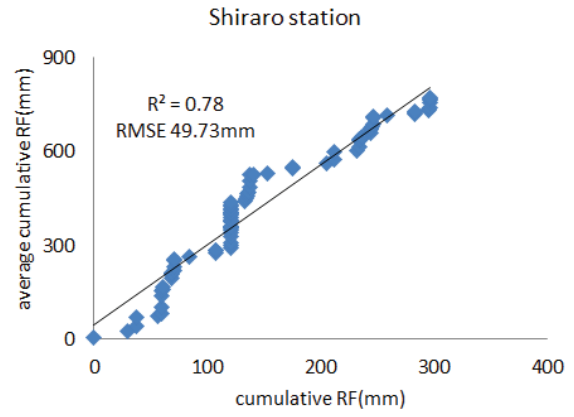
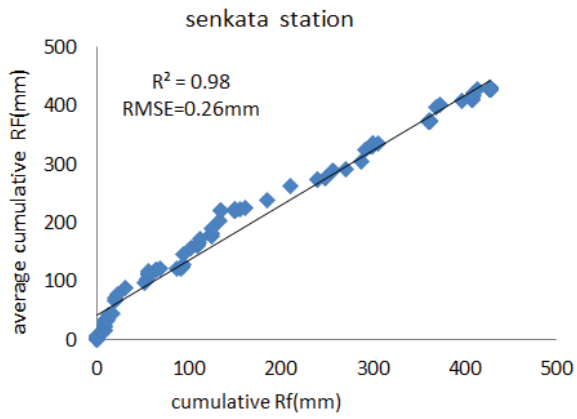
Chercher station



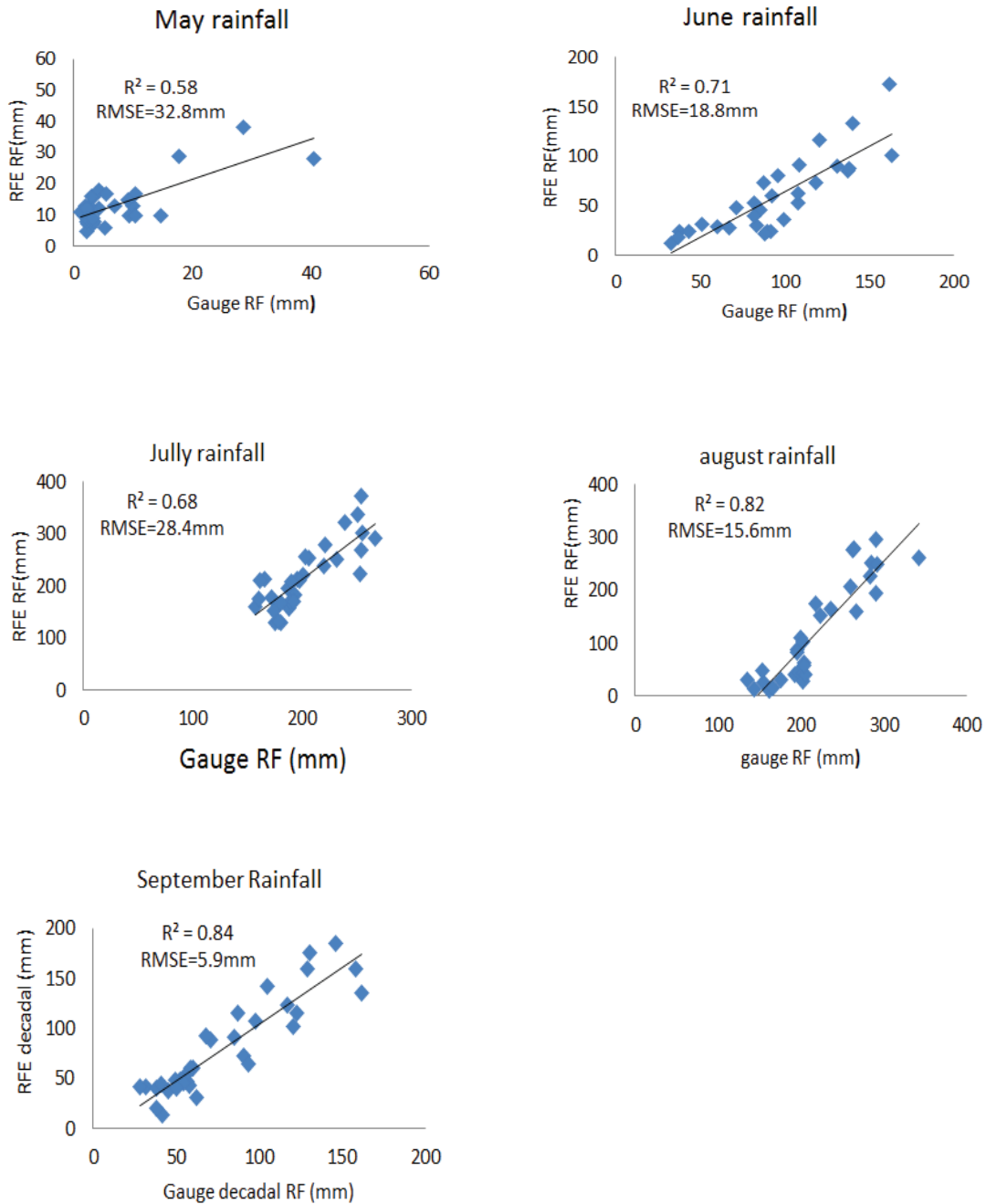
E.hamus station



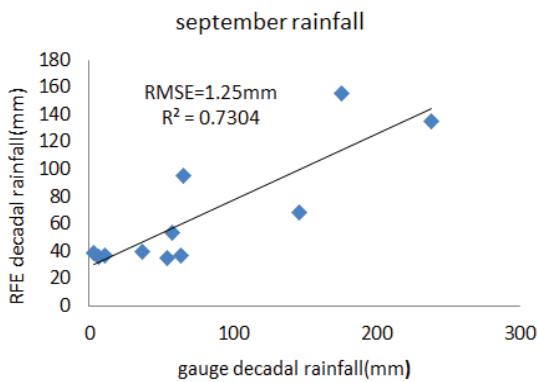
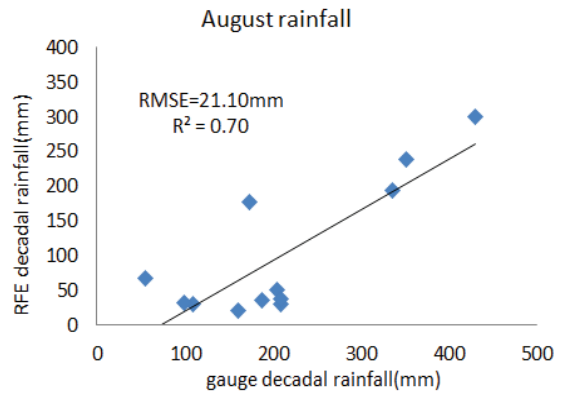
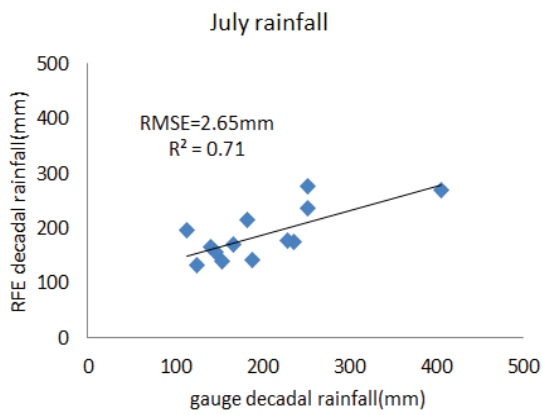
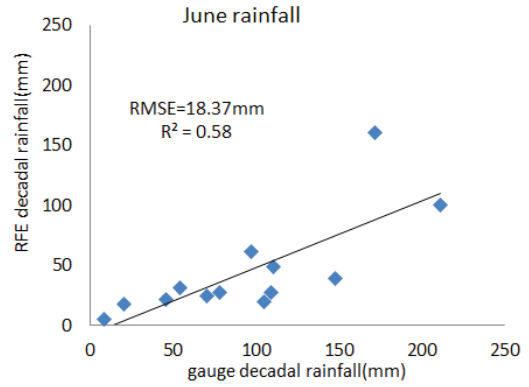
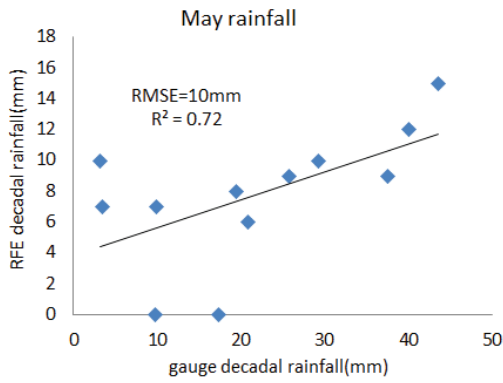




Appendix-C: - Scattered plot for pixel to pixel comparison of TAMSAT with in-situ gauge rainfall in Tigray region.



Appendix-D: - Scattered plot for Point to pixel comparison of TAMSAT with in-situ gauge rainfall in Tigray region.



Appendix-E: - Evapotranspiration trends for wheat and barley in the area.

